

1 **A genetically-encoded fluorescent sensor enables rapid**
2 **and specific detection of dopamine in flies, fish, and mice**

3 Fangmiao Sun^{1,2,*}, Jianzhi Zeng^{1,2,3,*}, Miao Jing^{1,2,3,*}, Jingheng Zhou⁴, Jiesi Feng^{1,2,3},
4 Scott F. Owen⁵, Yichen Luo¹, Funing Li⁶, Takashi Yamaguchi⁷, Zihao Yong⁸, Yijing Gao⁷,
5 Wanling Peng^{9,10}, Lizhao Wang¹¹, Siyu Zhang¹¹, Jiulin Du^{6,12}, Dayu Lin^{7,13,14}, Min Xu^{9,10},
6 Anatol C. Kreitzer^{5,15}, Guohong Cui⁴, Yulong Li^{1,2,3}

7

8

9 ¹State Key Laboratory of Membrane Biology, Peking University School of Life Sciences,
10 Beijing 100871, China

11 ²PKU-IDG/McGovern Institute for Brain Research, Beijing 100871, China

12 ³Peking-Tsinghua Center for Life Sciences, Beijing 100871, China

13 ⁴Laboratory of Integrative Neuroscience, National Institute on Alcohol Abuse and
14 Alcoholism, National Institutes of Health, Rockville, MD, USA

15 ⁵Gladstone Institutes, San Francisco, CA 94158, USA

16 ⁶Institute of Neuroscience, State Key Laboratory of Neuroscience, CAS Center for
17 Excellence in Brain Science and Intelligence Technology, Shanghai Institutes for
18 Biological Sciences, Chinese Academy of Sciences, Shanghai, China

19 ⁷Neuroscience Institute, New York University School of Medicine, New York, NY, USA

20 ⁸College of Biological Sciences, China Agricultural University, Beijing 100193, China

21 ⁹Chinese Academy of Sciences Center for Excellence in Brain Science and Intelligence
22 Technology, Chinese Academy of Sciences, Shanghai 200031, China

23 ¹⁰Institute of Neuroscience, Chinese Academy of Sciences, Shanghai 200031, China

24 ¹¹Shanghai Jiao Tong University School of Medicine, Shanghai 200025, China

25 ¹²University of Chinese Academy of Sciences, Beijing, China

26 ¹³Department of Psychiatry, New York University School of Medicine, New York, NY,
27 USA

28 ¹⁴Center for Neural Science, New York University, New York, NY, USA

29 ¹⁵Gladstone Institutes, San Francisco, CA, USA; Department of Neurology, UCSF, San
30 Francisco, CA, USA; Kavli Institute for Fundamental Neuroscience, UCSF, San
31 Francisco, CA, USA; UCSF Weill Institute for Neurosciences, UCSF, San Francisco,
32 CA, USA; Department of Physiology, UCSF, San Francisco, CA 94158, USA

33 *These authors contributed equally to this work

34

35 Manuscript correspondence:

36 Yulong Li (yulongli@pku.edu.cn)

37

38

39 **Abstract**

40

41 **Dopamine (DA) is a central monoamine neurotransmitter involved in many**
42 **physiological and pathological processes. A longstanding yet largely unmet goal is**
43 **to measure DA changes reliably and specifically with high spatiotemporal precision,**
44 **particularly in animals executing complex behaviors. Here we report the**
45 **development of novel genetically-encoded GPCR-Activation-Based-DA (GRAB_{DA})**
46 **sensors that enable these measurements. In response to extracellular DA rises,**
47 **GRAB_{DA} sensors exhibit large fluorescence increases ($\Delta F/F_0 \sim 90\%$) with sub-second**
48 **kinetics, nanomolar to sub-micromolar affinities, and excellent molecular specificity.**
49 **Importantly, GRAB_{DA} sensors can resolve a single-electrical-stimulus evoked DA**
50 **release in mouse brain slices, and detect endogenous DA release in the intact brains**
51 **of flies, fish, and mice. In freely-behaving mice, GRAB_{DA} sensors readily report**
52 **optogenetically-elicited nigrostriatal DA release and depict dynamic**
53 **mesoaccumbens DA changes during Pavlovian conditioning or during sexual**
54 **behaviors. Thus, GRAB_{DA} sensors enable spatiotemporal precise measurements of**
55 **DA dynamics in a variety of model organisms while exhibiting complex behaviors.**

56

57 Introduction

58

59 Dopamine is a crucial monoamine neurotransmitter in both vertebrates and
60 invertebrates. In the vertebrate central nervous system, DA regulates a wide
61 range of complex processes, including reward signaling (Schultz, 2016; Wise,
62 2004), reinforcement learning (Holroyd and Coles, 2002), attention (Nieoullon,
63 2002), motor control (Graybiel et al., 1994), arousal (Kume et al., 2005; Wisor
64 et al., 2001), and stress (Abercrombie et al., 1989). In the human brain,
65 impaired DA transmission is associated with neuropsychiatric disorders and
66 neurodegenerative diseases, including attention deficit hyperactivity disorder
67 (Cook Jr et al., 1995), schizophrenia (Howes and Kapur, 2009) and Parkinson's
68 disease (Lotharius and Brundin, 2002). Moreover, psychostimulants, such as
69 cocaine and amphetamine, exert their addictive effects by targeting
70 components in the DA signaling pathway and by altering extracellular DA levels
71 (Di Chiara and Imperato, 1988; Giros et al., 1996; Hernandez and Hoebel, 1988;
72 Ritz et al., 1987).

73

74 Despite many important roles that DA plays in both physiological and
75 pathological processes, precise measurements of the spatial and temporal
76 patterns of DA release during complex behaviors are lacking. This gap in
77 understanding due in large part to the limitation associated with existing
78 methods for the real-time detection of endogenous DA release in the intact brain.
79 Historically, intracerebral microdialysis has served as the gold standard for
80 quantitative measurements of extracellular DA concentration. However, the
81 relative slow sampling rate afforded by microdialysis is not well suited to detect
82 dynamic changes in DA levels during complex and rapidly evolving behaviors,
83 such as those that characterize social affiliation (Tidey and Miczek, 1996),
84 aggression (van Erp and Miczek, 2000), and mating (Pfaus et al., 1990a, b).
85 Fast-scan cyclic voltammetry (FSCV) is a temperamental electrochemical
86 method that can measure changes in extracellular DA concentrations with 10-
87 ms temporal resolution (Robinson et al., 2008; Rodeberg et al., 2017). However,
88 because FSCV requires oxidization of DA molecules, it is difficult to distinguish
89 DA from other structurally similar transmitters, such as norepinephrine (NE)
90 (Robinson et al., 2003). Moreover, both microdialysis and FSCV require
91 implantation of a relatively large probe or electrode (approximately 70-300 μm
92 in diameter) into a specific brain region, which precludes the ability to obtain
93 spatially precise measurements of endogenous DA release (Jaquins-Gerstl and
94 Michael, 2015).

95

96 In lieu of direct measurements of extracellular DA, indirect methods, for
97 example, measuring the activity of dopaminergic neurons (DANs) or the
98 activation of DA receptor downstream targets, have also been used to
99 approximate the dynamics of DA release. Genetic expression of a presynaptic
100 tethered Ca^{2+} indicator in DANs has been used to indicate potential
101 compartmentalized DA signals in the *Drosophila* olfactory pathway (Cohn et al.,
102 2015). However, given the highly complex regulation of presynaptic Ca^{2+} , the
103 nonlinear relationship between intracellular Ca^{2+} and transmitter release, as
104 well as the active uptake of extracellular DA by transporters, it is difficult to
105 quantitatively translate Ca^{2+} signals precisely into extracellular DA levels. Cell-
106 based DA reporters, such as CNiFERs (Muller et al., 2014), use transplated
107 HEK293 cells constitutively expressing DA receptors together with an
108 intracellular Ca^{2+} indicator to couple extracellular DA signals with the
109 fluorescence increase. However, This approach requires cell transplantation,
110 which may limit the broad usage of this method. Moreover, CNiFERs are not
111 spatially sensitive to synaptically released DA and thus may be limited to
112 measurements of volumetric transmission of DA. Finally, the TANGO assay and
113 their next-generation versions (Barnea et al., 2008; Inagaki et al., 2012; Kim et
114 al., 2017; Lee et al., 2017) have been used to measure endogenous DA release
115 by coupling the β -arrestin signaling pathway to reporter gene expression.
116 Although this approach enables the cell-type specific expression of the DA
117 reporter and is suitable for *in vivo* measurements, the long signal amplification
118 time (on the order of hours) required for this assay precludes the ability to
119 monitor rapid, physiologically relevant dynamics of DA signaling in real time.

120

121 Here, we report the development of novel, genetically-encoded sensors that
122 enable direct, rapid, sensitive, and cell-type specific detection of extracellular
123 DA. These sensors, which we call GRAB_{DA} sensors, were engineered by
124 coupling a conformationally sensitive circular-permuted EGFP (cpEGFP) to a
125 selected human DA receptor. Through iterative engineering and optimization,
126 we yielded two GRAB_{DA} sensors: GRAB_{DA1m}, with medium DA affinity ($\text{EC}_{50} \sim$
127 130 nM); and GRAB_{DA1h}, with high DA affinity ($\text{EC}_{50} \sim 10$ nM). We show that
128 these two newly developed GRAB_{DA} sensors enable real-time detection of
129 endogenous DA in acute brain slices of mice and in the intact brains of versatile
130 animal models including flies, fish, and mice.

131

132

133

134 **Results**

135

136 **Development and initial characterization of GRAB_{DA} sensors**

137

138 To develop a genetically encoded sensor for DA, we sought to engineer
139 naturally evolved DA receptors to couple a conformationally sensitive cpEGFP.
140 We hypothesized that upon DA binding, the conformational changes in the
141 receptor could alter the arrangement of the associated cpEGFP, resulting in a
142 DA-dependent change in fluorescence. Indeed, a similar strategy was recently
143 applied in creating the genetically encoded acetylcholine sensor GACH (Miao
144 Jing et al., 2018), suggesting that this strategy could potentially be expanded
145 to generate DA sensors.

146

147 We used a three-step approach to engineer and optimize GRAB_{DA} sensors (Fig.
148 1A-C): First, as the third intracellular loop (ICL3) of the G protein-coupled
149 receptor (GPCR) links transmembrane V and VI that are thought to undergo
150 large conformational changes upon ligand binding (Kruse et al., 2013), a
151 cpEGFP was first inserted into the ICL3 of all five subtypes of human dopamine
152 receptors (DRs); we subsequently focused on the D₂R-cpEGFP chimera due to
153 its superior membrane trafficking and relatively high affinity for DA (Beaulieu
154 and Gainetdinov, 2011; Missale et al., 1998) (Fig. S1A,B). In the second step,
155 the position of the cpEGFP insertion within the ICL3, and individual amino-acids
156 in the linker region between cpEGFP and D₂R were systematically screened
157 (Fig. 1A,B). Finally, mutations at residues critical for receptors affinity for DA
158 (Sung et al., 2016) were further introduced to expand the sensor's response
159 range (Fig. 1C). After screening a total of more than 432 variants, we chose two,
160 GRAB_{DA1m} and GRAB_{DA1h}, both of which have a ~90% maximal $\Delta F/F_0$ response
161 to the application of saturating levels of DA (Fig. 1B,E), but differ by an order of
162 magnitude with respect to affinity for DA (130 nM for GRAB_{DA1m} and 10 nM for
163 GRAB_{DA1h}) (Fig. 1C). We also generated a corresponding mutant variant of
164 each sensor (GRAB_{DA1m-mut} and GRAB_{DA1h-mut}) by introducing C118A and
165 S193N double mutations in the receptor's putative DA-binding pocket in order
166 to abolish the DA binding (Chien et al., 2010b; Wang et al., 2018) (Fig. S1D).
167 These so-called "dead" mutants exhibited no DA-induced change in
168 fluorescence compared with GRAB_{DA1m} and GRAB_{DA1h} (Fig. 1D).

169

170 We next characterized the properties of the two GRAB_{DA} sensors in detail in

171 cultured HEK293T cells. Both GRAB_{DA1m} and GRAB_{DA1h} trafficked efficiently to
172 the plasma membrane of HEK293T cells (Fig. 1D and Fig. S1C). Cells
173 expressing GRAB_{DA1m} and GRAB_{DA1h} exhibited robust fluorescence increases
174 upon bath application of DA (Fig. 1D-F). Notably, the DA-induced fluorescence
175 increase was completely blocked by the co-application of the D₂R antagonist
176 haloperidol (Halo) (Sokoloff et al., 1990), confirming the molecular specificity of
177 these sensors (Fig. 1E). Both mutant forms of GRAB_{DA} sensors trafficked
178 normally to the plasma membrane, similar to GRAB_{DA1m} and GRAB_{DA1h} (Fig.
179 1D and Fig. S1C), albeit with no detectable fluorescence increase in response
180 to DA application (Fig. 1D,E). To characterize the response kinetics of
181 GRAB_{DA1m} and GRAB_{DA1h}, agonists or antagonists at high concentrations were
182 locally applied to HEK293T cells expressing these sensors via a rapid perfusion
183 system (Fig. 1F,G). Both GRAB_{DA1m} and GRAB_{DA1h} showed rapid fluorescence
184 increases (on rate) in response to DA application, with a time constant of ~100
185 ms (60 ± 10 ms for GRAB_{DA1m} and 140 ± 20 ms for GRAB_{DA1h}, respectively),
186 implying that GRAB_{DA} sensors are suitable for tracking rapid DA dynamics. The
187 fluorescence decrease (off rate) of the GRAB_{DA} sensors in response to
188 applications of the antagonist Halo is slower in GRAB_{DA1h} (2.5 ± 0.3 s)
189 compared with GRAB_{DA1m} (0.7 ± 0.06 s), consistent with the differences in
190 affinity (Fig. 1G). We also measured the photostability of GRAB_{DA1m} and
191 GRAB_{DA1h} in HEK293T cells. Under confocal laser illumination, both GRAB_{DA}
192 sensors were significantly more photostable than a membrane targeted EGFP
193 or the glutamate sensor iGluSnFR (Marvin et al., 2013) (Fig. S2), suggesting
194 that these new DA sensors are suitable for long-term measurements of DA
195 dynamics.

196

197 We also tested the specificity of GRAB_{DA} sensors for DA comparing with other
198 neurotransmitters. HEK293T cells expressing GRAB_{DA} sensors were
199 sequentially perfused with solutions containing different neurotransmitters (Fig.
200 1H and Fig. S3; all were applied at 1 μ M concentration). Again, bath application
201 of DA induced robust fluorescence increases in both GRAB_{DA1m}- and
202 GRAB_{DA1h}-expressing cells, and these signals were completely blocked by co-
203 application of D₂R antagonists Halo or eticlopride (Etic), but not by the D₁R
204 antagonist SCH-23390 (SCH). In contrast, applications of various other
205 neurotransmitters, including serotonin (5-HT), histamine (His), glutamate (Glu),
206 GABA, adenosine (Ade), acetylcholine (ACh), tyramine (Tyr), octopamine (Oct),
207 glycine (Gly), or the DA precursor L-DOPA, did not elicit any detectable
208 fluorescence changes (Fig. 1H and Fig. S3). We found that NE application
209 evoked a small yet significant increase in fluorescence in both GRAB_{DA1m}- and
210 GRAB_{DA1h}-expressing cells, although this increase was considerable smaller

211 than the response elicited by DA applied at the same concentration (for
212 GRAB_{DA1m}, the $\Delta F/F_0$ in response to NE is 26% of that to DA). Further
213 characterization of the affinity of GRAB_{DA1m} or GRAB_{DA1h} to both DA and NE
214 revealed a 10-fold higher affinity to DA against NE (Fig. 1H and Fig. S3), as
215 expected from the specificity of native human D₂R to DA and NE (Lanau et al.,
216 1997b). Overall, GRAB_{DA1m} and GRAB_{DA1h} sensors show rapid and highly
217 sensitive responses to physiological ranges of DA with little or no sensitivity to
218 almost all other neurotransmitters tested here.

219

220 Does ectopic expression of GRAB_{DA} sensors elicit unintended signaling by
221 coupling to GPCR's downstream pathways? To examine this, we separately
222 tested the coupling efficacies of GRAB_{DA} sensors to either G protein- or β -
223 arrestin-dependent pathways that are known to be downstream of activated
224 D₂R (Beaulieu and Gainetdinov, 2011). It is well established that the coupling
225 of a G protein with its cognate GPCR significantly increases the receptor's
226 binding affinity for its ligand (Kruse et al., 2013). We therefore used pertussis
227 toxin (PTX), which potently and selectively blocks the coupling between Gi
228 proteins and GPCRs, such as D₂R (Burns, 1988). In cells expressing either
229 GRAB_{DA1m} or GRAB_{DA1h}, co-expression of PTX did not significantly alter the
230 sensors' affinity for DA, indicating that GRAB_{DA} sensors do not couple
231 extensively to Gi proteins (Fig. 1I). On the other hand, if the DA-binding of
232 GRAB_{DA} sensors activates the β -arrestin-dependent pathway, the resulting
233 internalization of sensors would reduce the fluorescence at the plasma
234 membrane of HEK293T cells (Luttrell and Lefkowitz, 2002). However, we
235 observed stable membrane fluorescence of the GRAB_{DA} sensor-expressing
236 cells throughout a 2-hour exposure to DA at a saturation concentration (100
237 μ M), suggesting no detectable activation of β -arrestin-dependent signaling
238 under these conditions (Fig. 1J). Collectively, these data suggest that GRAB_{DA}
239 sensors do not engage these major downstream GPCR-mediated signaling
240 pathways.

241

242 **Characterization of GRAB_{DA} in cultured neurons**

243

244 We next evaluated the expression pattern and functional properties of GRAB_{DA}
245 sensors in cultured rat cortical neurons. After 48h expression, both GRAB_{DA1m}
246 and GRAB_{DA1h} showed basal fluorescence signals in transfected neurons, with
247 the brightest signal in the plasma membrane of somas and neurites, indicated
248 by the colocalization with a membrane marker RFP-CAAX (Hancock et al.,

249 1991) (Fig. 2A,B and Fig. S4). In addition, co-expression of the GRAB_{DA}
250 sensors with the postsynaptic (PSD95-RFP) or presynaptic (SYP-RFP)
251 markers revealed that GRAB_{DA} sensors were distributed throughout the entire
252 membrane in dendritic shafts, spines, axons and axonal boutons, suggesting
253 the suitability of GRAB_{DA} sensors to detect DA dynamics in sub-neuronal
254 compartments (Fig. 2B and Fig. S4). As in HEK293T cells, DA application in
255 transfected cultured neurons induced dose-dependent fluorescence increases
256 in both GRAB_{DA1m}- and GRAB_{DA1h}-expressing neurons with a similar maximum
257 $\Delta F/F_0$ of ~90%, and with an EC₅₀ of ~170 nM and ~8 nM for GRAB_{DA1m} and
258 GRAB_{DA1h}, respectively (Fig. 2C-E). Moreover, the specificity of both GRAB_{DA}
259 sensors for DA was similar in cultured neurons compared to HEK 293T cells
260 (Fig. 2F). Finally, no detectable decrease of surface fluorescence signals of
261 GRAB_{DA} sensors-expressing cells was observed in response to a 2-h
262 continuous application of DA at a saturation concentration (100 μ M) (Fig. 2G),
263 suggesting that GRAB_{DA} sensors were not internalized over this time frame.
264 Collectively, these data demonstrate that GRAB_{DA} sensors can monitor DA
265 signals with high sensitivity and specificity in cultured rat cortical neurons.

266

267 **Characterization of GRAB_{DA} in acute brain slices**

268

269 A crucial issue is whether GRAB_{DA} sensors are sufficiently sensitive to detect
270 and monitor endogenous DA release in native brain tissue. To begin to resolve
271 this issue, we injected AAVs carrying either GRAB_{DA1m} or GRAB_{DA1h} into the
272 nucleus accumbens (NAc) of mice, then prepared acute brain slices containing
273 NAc two weeks later. Post hoc visualization in fixed brain slices revealed that
274 the fluorescent signal of GRAB_{DA} sensors could be detected in the NAc region
275 of virus-injected mice, and the signal was in close proximity to putative DA-
276 releasing fibers that were immunoreactive for tyrosine hydroxylase (TH) (Fig.
277 3A). Electrical stimulation within NAc core elicited robust and time-locked
278 fluorescence increases in both GRAB_{DA1m}- and GRAB_{DA1h}-expressing neurons
279 (Fig. 3A-C). Increasing the number of stimulation pulses or stimulation
280 frequency resulted in a progressive increase in the intensity of evoked
281 fluorescence signals in neurons expressing GRAB_{DA1m} or GRAB_{DA1h} (Fig. 3B,C).
282 These stimulus-evoked fluorescent signals reached plateau levels at high
283 stimulation frequency with large stimulation number (e.g. more than 50 pulses)
284 in GRAB_{DA1h} expressing neurons, presumably due to saturation of the sensor
285 arising from GRAB_{DA1h}'s high affinity for DA. The rise times of stimulus-evoked
286 fluorescence signals were fast in both GRAB_{DA1m}- and GRAB_{DA1h}-expressing
287 neurons (Fig. 3D), whereas the decay time of fluorescent signals in GRAB_{DA1h}

288 expressing neurons was slower than that in neurons expressing GRAB_{DA1m} (Fig.
289 3D), consistent with the DA affinity and response kinetics measured in cultured
290 cells (see Fig. 1C,G). Repeated electrical stimuli delivered at 5-minute intervals
291 evoked reproducible fluorescence responses, indicating the reliability and
292 stability of GRAB_{DA1m} and GRAB_{DA1h} in reporting multiple DA releasing events
293 (Fig. 3E). Bath application of the D₂R antagonist Halo abolished the electrically
294 stimuli-induced fluorescence responses in either GRAB_{DA1m}- or GRAB_{DA1h}-
295 expressing neurons (Fig. 3F), verifying the sensor's specificity when expressed
296 in brain slices. Collectively, both GRAB_{DA1m} and GRAB_{DA1h} enable sensitive and
297 specific detection of endogenous DA dynamics in acute mouse brain slices.

298

299 **Imaging DA dynamics in *Drosophila***

300

301 We next examined the ability of GRAB_{DA} sensors to detect physiologically
302 relevant DA dynamics in living animals. We selected the fly as an initial test of
303 our sensors, as DA plays a key role in the fly brain, serving as a critical teaching
304 signal in olfactory-associative learning (Burke et al., 2012; Heisenberg, 2003;
305 Liu et al., 2012; Schwaerzel et al., 2003). Transgenic UAS-GRAB_{DA1m} flies were
306 generated and first crossed with TH-GAL4 to express GRAB_{DA1m} specifically in
307 DANs. Two-photon imaging methods were used to study odor-evoked DA
308 signals in the mushroom body (MB) in living flies (Fig. 4A). We found that the
309 odorant isoamyl acetate (IA) elicited a time-locked fluorescence increase in the
310 MB, most prominently in the β' lobes, and this IA-evoked response was blocked
311 by Halo application. In contrast, no IA-evoked fluorescence response was
312 observed in flies expressing GRAB_{DA1m-mut} (Fig. 4B). To further test the signal
313 specificity, we use the C305a-GAL4 line to express GRAB_{DA1m} in Kenyon cells
314 which receives direct input from DANs (Aso et al., 2010). Comparing wild-type
315 (WT) control flies and TH-deficient flies (Cichewicz et al., 2017), which lack DA
316 synthesis in the CNS. Compared with WT flies, we observed no detectable IA-
317 evoked GRAB_{DA1m} fluorescence increase was observed in TH-deficient flies
318 (Fig. 4B,C). We also examined whether the ectopic expression of GRAB_{DA}
319 sensors may alter physiological properties, such as the neuronal excitability.
320 We observed no significant difference between GRAB_{DA} sensors-expressing
321 and non-expressing DANs or Kenyon cells with respect to odor-evoked Ca²⁺
322 signals (Fig. S5), suggesting that expression of the sensor does not alter odor-
323 evoked responses in neurons in the fly brain.

324

325 To further characterize the sensitivity and kinetics of GRAB_{DA1m} *in vivo*, we

326 electrically stimulated MB DANs while simultaneously monitoring the
327 corresponding fluorescence signals (Fig. 4D,E). We found that GRAB_{DA1m}-
328 expressing DANs exhibited a reproducible fluorescence increases in response
329 to repeated trains of electrical stimuli delivered at various frequencies, and even
330 a single stimulus was sufficient to elicit a measurable increase in fluorescence
331 (Fig. 4D,E). In contrast, similar electrical stimulation did not evoke any
332 detectable fluorescence increase in flies expressing GRAB_{DA1m-mut} (Fig. 4D,E).
333 With the increase of pulse number delivered at 20 Hz, fluorescence signals of
334 GRAB_{DA1m} increased progressively and reached a plateau of peak $\Delta F/F_0$ of ~35%
335 after 10 pulses (Fig. 4F-H). The fluorescence responses evoked by electrical
336 stimulation exhibited sub-second kinetics, with on and off time constants of 0.07
337 ± 0.01 s and 0.39 ± 0.05 s, respectively (Fig. 4I), indicating the suitability of
338 GRAB_{DA1m} for monitoring endogenous transient DA signals. Consistent with the
339 odor-evoked fluorescence increase, application of Halo completely blocked the
340 fluorescence increases elicited by electrical stimuli (Fig. 4J,K), confirming the
341 sensor's specificity.

342

343 The DA transporter (DAT), which is a highly conserved protein across insects
344 and vertebrates, is responsible for the reuptake of DA from extracellular space
345 for subsequent reuse, and is the primary target of many drugs of abuse (Bainton
346 et al., 2000; Ritz et al., 1987). Impairing DAT function results in sustained
347 elevation of extracellular DA levels (Fig. 4L) (Bainton et al., 2000; Ritz et al.,
348 1987). To determine whether our sensor could detect changes in extracellular
349 DA arising from manipulation of the DAT, we applied cocaine, a psychostimulant
350 drug that blocks DAT. Cocaine significantly potentiated the odor-evoked
351 fluorescence increase of GRAB_{DA1m} expressed in MB DANs, and this cocaine-
352 potentiated response was accompanied by a prolonged decay in the
353 fluorescence signal (Fig. 4M-O). Genetically knocking down the expression of
354 DAT selectively in DANs phenocopied the effect of cocaine administration (Fig.
355 4M-O), confirming the ability of GRAB_{DA1m} to measure the dynamic regulation
356 of DA release and reuptake *in vivo*. Together with our results described above,
357 these data demonstrated that GRAB_{DA} sensors have the sensitivity, fast
358 kinetics, and specificity to report *in vivo* DA dynamics in genetically-defined
359 neurons in the intact brain of living flies.

360

361 **Imaging DA release in the intact zebrafish brain**

362

363 Zebrafish larvae have an optically transparent brain and is capable of

364 performing a wide range of behaviors, affording a powerful system to explore
365 the structure and function of the vertebrate brain at cellular resolution in a
366 behavioral framework. To test the feasibility of using GRAB_{DA} sensors in
367 imaging DA dynamics in zebrafish larvae, we generated the transgenic line
368 Tg(elval3:GRAB_{DA1m}/DAT:TRPV1-TagRFP), in which GRAB_{DA1m} was
369 expressed pan-neuronally throughout the brain, and TRPV1-TagRFP was
370 expressed specifically in DANs to enable their chemogenetic activation by
371 capsaicin (Fig. 5A). We first applied DA to the fish, and observed fluorescence
372 increases in GRAB_{DA1m}-expressing neurons in the head, which were blocked
373 by co-application of antagonist Halo, suggesting the specificity of GRAB_{DA} (Fig.
374 5B-D).

375

376 Next, we hope to track the dynamics of endogenous DA signals in zebrafish
377 larvae. We previously reported that the optic tectum of zebrafish larvae receives
378 synaptic input from pretectal DANs (Shang et al., 2015), advancing the tectum
379 as a potential site to monitor DA release. We therefore performed confocal
380 imaging of GRAB_{DA1m}-expressing tectal neurons in the live transgenic zebrafish
381 larvae (Fig. 5E). Repeated application of capsaicin (five 100-ms puffs delivered
382 with a 1-min interval) caused the progressive increase in the fluorescence
383 signals in the tectal neuropil (Fig. 5F-H). The capsaicin-induced fluorescence
384 increase was again abolished by the application of Halo (Fig. 5F-H), confirming
385 that the response was specifically due to GRAB_{DA1m} activation. Thus, the
386 GRAB_{DA1m} is well suited to report *in vivo* DA dynamics in the brain of zebrafish
387 larvae.

388

389 **Combining optogenetics with GRAB_{DA} to measure the dynamics of DA in** 390 **freely moving mice**

391

392 To test the ability of GRAB_{DA} sensors to report DA dynamics in specific circuits
393 in the mouse brain *in vivo*, we focused on DANs located in the substantia nigra
394 pars compacta (SNc) that project to the dorsal striatum (Str). This nigrostriatal
395 pathway is implicated in complex behavioural functions including motivation,
396 reward, and learning (Balleine et al., 2007; Da Silva et al., 2018; Howe and
397 Dombeck, 2016). We virally expressed DIO-C1V1 (Yizhar et al., 2011) in the
398 SNc of TH-Cre mice, permitting selective optogenetic activation of DANs.
399 Additionally, we virally co-expressed GRAB_{DA1m} and tdTomato in the dorsal
400 striatum, allowing us to simultaneously monitor DA release using the green
401 (GRAB_{DA1m}) channel while detecting movement-related fluorescence artefacts

402 using the red (tdTomato) channel (Fig. 6A,B, see methods for detail). In free
403 moving mice, the ratio of GRAB_{DA1m} to tdTomato fluorescence was elevated
404 upon the administration of methylphenidate, a known DAT blocker (Volkow et
405 al., 1999) (Fig. 6C, top), and was suppressed by subsequent administration of
406 Etic (Fig. 6C, top), a D₂R blocker, implying the ability of GRAB_{DA} sensors in
407 reporting DA dynamics to pharmacological treatments. Interestingly, we
408 observed fluctuations in the ratio of GRAB_{DA1m} to tdTomato fluorescence that
409 likely reflect the spontaneous DA release during the animal movements
410 (Balleine et al., 2007; Da Silva et al., 2018; Howe and Dombeck, 2016), as they
411 were prolonged during methylphenidate application and largely diminished by
412 Etic administration (Fig. 6C, bottom).

413

414 Combining optogenetic stimulation and fiber photometry in freely moving mice,
415 we observed that C1V1-evoked activation of DANs in the SNc generated a
416 time-locked transient fluorescence increase in the dorsal striatum specific to the
417 GRAB_{DA1m} channel (Fig. 6D), consistent with the evoked DA release from SNc
418 DAN terminals. Systemic administration of the DA transporter blocker
419 methylphenidate significantly prolonged the decay of optogenetically-evoked
420 GRAB_{DA1m} fluorescence responses in the dorsal striatum (Fig. 6D,E).
421 Furthermore, administration of D₂R antagonist Etic largely abolished the
422 response (Fig. 6D,F). Therefore, the GRAB_{DA}- and C1V1- based all-optical
423 approach is effective for monitoring spontaneous and optogenetically-evoked
424 DA release in the nigrostriatal pathway of mice.

425

426 **Bi-directional modulation of DA dynamics in the nucleus accumbens** 427 **(NAc) during Pavlovian conditioning**

428

429 In addition to the nigrostriatal pathway, the dopaminergic projection from the
430 ventral tegmental area (VTA) to the nucleus accumbens (NAc) regulates a
431 variety of important functions including the reinforcement learning (Daw and
432 Tobler, 2013; Glimcher, 2011; Gonzales et al., 2004), wherein an animal learns
433 to associate an initially neutral sensory cue, such as a short tone burst, with an
434 ensuing reward or punishment. Previous studies show that DANs in the VTA
435 fire phasically to unpredicted rewards or reward-predicting cues and, with
436 conditioning, the reward-evoked response diminishes as it becomes fully
437 predicted by the cue (Bayer and Glimcher, 2005; Schultz, 2006; Schultz et al.,
438 1997). To test whether our sensor can detect behaviourally relevant changes in
439 endogenous DA release, we first expressed GRAB_{DA1h} in the NAc of head-fixed,

440 water-restricted mice and trained them to associate a brief auditory cue with
441 subsequent delivery of a liquid sucrose water reward (Fig. 7A). Each mouse
442 experienced two distinct auditory cues, one that predicted delivery of a reward
443 within a variable delay of 500-1500 ms after the end of the cue, as well as a
444 second, randomly interleaved control cue (No Water, N.W.) that was not
445 associated with water reward. Mice were trained daily for ~10 days, and the
446 GRAB_{DA1h} signal was recorded using *in vivo* fiber photometry in both the early
447 and late stages of training. Consistent with the expected DA signaling in this
448 classical paradigm, elevations in the GRAB_{DA1h} fluorescent signal aligned to
449 reward delivery in every mouse, immediately in the first session without
450 requiring training (Fig. 7C,E). After 6-10 days of training, mice selectively
451 learned to associate the reward-predictive cue with delivery of reward.
452 Consistent with the established reward prediction error theory of DA function,
453 DA signals emerged in trained mice in response to the reward-predicting cue
454 before the delivery of the reward (Fig. 7B,D-F). These results demonstrate that
455 the signal-to-noise and temporal resolution of GRAB_{DA1h} is sufficient to detect
456 physiologically relevant DA signaling *in vivo* in awake, behaving mice.
457 Furthermore, these results serve to validate the GRAB_{DA1h} recorded DA signals
458 by anchoring them to decades of established basal ganglia and the physiology
459 of DA neurons.

460

461 In addition to transient elevations in DA signal in response to unexpected
462 reward, DA neuron firing dips briefly in response to aversive stimuli (Brooks and
463 Berns, 2013; Schultz, 2007; Ungless et al., 2004). We expressed the lower
464 affinity GRAB_{DA1m} in the NAc of mice and trained them to associate a tone burst
465 with an ensuing reward (a drop of water), or a punishment (a brief air puff to the
466 face) to test whether our sensor can detect bi-directional changes in DA tone.
467 During training, mice learned the association between an auditory cue and
468 several outcomes (Fig. 7A). *In vivo* fiber photometry recording of GRAB_{DA}
469 signals revealed that during early stages of training, reward or punishment
470 delivery triggered a robust increase or decrease in the fluorescence signal in
471 the NAc (Fig. 7G,H). Over the course of training, the magnitude of this reward-
472 evoked response decreased, while a response of similar sign developed to the
473 associated cue (Fig. 7G,H). In summary, the GRAB_{DA} sensor can be used to
474 report the dynamic bi-directional changes in DA release over the course of
475 Pavlovian conditioning.

476

477 **Monitoring DA release in the NAc of mice during male mating behaviors**

478

479 In contrast to the well-established involvement of DA in Pavlovian conditioning,
480 DA dynamics during naturally rewarding social behaviors (Berridge and
481 Robinson, 1998), such as courtship and mating, remains largely a subject of
482 debate. Microdialysis and voltammetric measurements have previously
483 revealed a relatively slow change in DA concentration during sexual behaviors:
484 DA levels in the male's NAc start to increase after a female is introduced into
485 his cage and continues to rise throughout the course of sexual behaviors and
486 ejaculation (~20 minutes), then slowly (~30 minutes) return to baseline after the
487 female is removed (Damsma et al., 1992; Mas et al., 1995; Pfaus et al., 1990b).
488 In contrast, a more recent study using FSCV showed that DA is transiently
489 released in the male's NAc when the female is introduced but few changes in
490 DA levels were detected during subsequent sexual behaviors (Robinson et al.,
491 2002; Robinson et al., 2001). To better understand DA dynamics during sexual
492 behaviors, we virally expressed GRAB_{DA1h} in the NAc of male mice and used
493 fiber photometry to record DA signals during sexual behaviors (Fig. 8A). Four
494 weeks after injection, a sexually receptive C57BL/6 female was introduced into
495 the home cage of the male mouse. Upon a female introduction, the male quickly
496 approached and investigated the female, and then initiated mounting within the
497 first minute. The GRAB_{DA1h} signals measured in the male's NAc acutely and
498 consistently increased with investigation of the female, mounting, intromission,
499 ejaculation, and penile grooming (Fig. 8B). When we aligned the GRAB_{DA1h}
500 signals with the manually annotated behaviors for each male, we observed that
501 fluorescence signals increased prior to the corresponding behavior, peaked at
502 the behavior's onset, and then gradually declined (Fig. 8C). Among all of the
503 sexual behaviors we annotated, the largest fluorescence increase occurred
504 during intromission and ejaculation (Fig. 8C,D). These results indicate that DA
505 in the NAc is acutely released during episodes of sexual behaviors and may
506 carry information regarding specific features of courtship and/or mating.

507

508 Discussion

509

510 Here we describe the development and characterization of a pair of novel
511 genetically-encoded sensors that enable specific, real-time detection of
512 endogenous DA dynamics in various *ex vivo* and *in vivo* preparations and model
513 systems. In acute mouse brain slices, GRAB_{DA} sensors were well suited to
514 monitor stimulus-evoked DA release in mesolimbic pathway. In flies, GRAB_{DA}
515 sensors were sufficiently sensitive to detect DA release in the MB triggered by
516 odorants presented at physiologically relevant concentrations, and could also
517 readily resolve DA release evoked by a single electrical stimulus. In transgenic
518 zebrafish, GRAB_{DA} sensors were able to report DA release in the optic tectum

519 in response to the chemogenetic activation of pretecal DANs. In mice,
520 combining optogenetic stimulation with GRAB_{DA} sensors enabled the
521 simultaneous optical manipulation and detection of DA signals *in vivo*. Finally,
522 GRAB_{DA} sensors revealed real-time DA dynamics in the NAc of freely behaving
523 mice as they underwent Pavlovian conditioning or engaged in sexual behaviors.

524

525 Compared to current methods used to measure DA release, our GRAB_{DA}
526 sensors described here exhibit several clear advantages. First, GRAB_{DA}
527 sensors are genetically-encoded by relatively small genes (~2 kb), making them
528 highly amenable to transgenic approaches and viral packaging. Second,
529 GRAB_{DA} sensors have high sensitivity to DA. In response to DA, GRAB_{DA1m} and
530 GRAB_{DA1h} sensors are capable of achieving maximal $\Delta F/F \sim 90\%$ with ~10 nM
531 and ~100 nM affinities, respectively. In contrast, conventional GPCR-based
532 FRET probes for detecting neurotransmitters are usually limited to a maximum
533 FRET signal changes of ~ 5% under optimal conditions, and less than that *in*
534 *vivo* (Villardaga et al., 2003; Ziegler et al., 2011). Third, GRAB_{DA} sensors have
535 high specificity to DA: A range of experimental approaches, including
536 application of multiple neurotransmitters and D₂R antagonists, perturbation of
537 DATs, or manipulation of DA synthesis pathways unequivocally support the
538 molecular specificity of GRAB_{DA} sensors for DA. Notably, similar to the human
539 D₂R upon which they are based, both GRAB_{DA} sensors have a 10-fold higher
540 affinity for DA than for NE (Lanau et al., 1997b); in contrast, FSCV is unable to
541 discriminate between these two catecholamines (Fox and Wightman, 2016;
542 Park et al., 2009). Finally, GRAB_{DA} sensors have extremely rapid response
543 kinetics: GRAB_{DA} sensors report increases in DA levels with a rise time of ≤ 100
544 ms (Fig. 1G, 3D and 4I). Although this response time of GRAB_{DA} sensors is
545 slower than voltammetry methods, it is still sufficiently rapid for reporting
546 physiologically relevant DA dynamics and share response kinetics similar to WT
547 GPCRs (Lohse et al., 2008), providing an accurate readout of their activation.

548

549 Because GRAB_{DA} sensors were engineered using the D₂R, a G_i-coupled GPCR,
550 a potential concern is that overexpressing the GRAB_{DA} sensors may
551 inadvertently activate pathways downstream of D₂R. However, several lines of
552 evidence argue against this possibility, including the negligible coupling
553 between GRAB_{DA} sensors and both G protein-dependent and arrestin-
554 dependent intracellular signaling pathways, alleviating this concern (Fig. 1I, 1J).
555 This lack of coupling is presumably due to the steric hindrance imposed by the
556 bulky cpEGFP moiety that replaces parts of the ICL3, which is the critical
557 position for G protein or arrestin to interact with the GPCR (Luttrell and

558 Lefkowitz, 2002; Neves et al., 2002). Consistent with minimal coupling between
559 GRAB_{DA} sensors and downstream signaling pathways, *in vivo* Ca²⁺ imaging
560 experiments using the Ca²⁺ sensor jRCaMP1a revealed no measurable
561 alteration in Ca²⁺ signaling in neurons of transgenic flies that overexpressing
562 GRAB_{DA} sensors (see Fig. S5).

563

564 In flies, DA signaling is critical for olfactory learning (Burke et al., 2012;
565 Heisenberg, 2003; Liu et al., 2012; Schwaerzel et al., 2003). Here show that
566 GRAB_{DA} sensors can be targeted to specific cells in the fly brain and used to
567 probe odor-evoked DA dynamics in the MB of the living fly in real-time. It is
568 reported that different types of DANs innervate different compartments of MBs,
569 and these different dopaminergic pathways may play distinct roles in appetitive
570 and aversive olfactory-dependent behaviors (Aso and Rubin, 2016; Cognigni et
571 al., 2017). The GRAB_{DA} sensors developed here create new opportunities for
572 exploring how distinct DA dynamics can correspond with specific compartments
573 in the MB of the intact fly, particularly as the animal engages in different
574 behavioral paradigms. Experiments in flies also illustrate the power of GRAB_{DA}
575 sensors to probe DAT function *in vivo* by directly measuring extracellular DA
576 level in real time. Similarly, we showed that GRAB_{DA} sensors readily respond
577 to DA transients in the intact brain of the zebrafish larvae, providing a robust
578 and convenient tool to examine DA dynamics in this classic vertebrate model
579 system.

580

581 In addition to the morphological distinctions that can be made between various
582 DANs in the mammalian CNS, breakthroughs in single-cell sequencing have
583 further divided these neurons into a wide variety of cell types with distinct
584 molecular features, suggesting high functional heterogeneity (Nair-Roberts et
585 al., 2008; Ungless and Grace, 2012). Therefore, genetically-encoded GRAB_{DA}
586 sensors provide a novel tool to explore patterns of DA release from genetically
587 distinct DAN types, thereby facilitating the understanding of how they may be
588 functionally specialized for different physiological and behavioral processes
589 (Lammel et al., 2014; Pignatelli and Bonci, 2015). In fact, GRAB_{DA} sensors
590 applied in the mouse faithfully reported the expected bi-directional regulation of
591 DA levels in the NAc during different forms of Pavlovian conditioning.
592 Consistent with the notion that DA can predict an anticipated reward (Schultz
593 et al., 1997), the GRAB_{DA} sensor detected a robust, phasic increase in DA
594 levels that shifted from reward onset to cue onset over the course of reward
595 learning. Conversely, in naïve animals, a transient decrease in DA levels was
596 triggered by the air puff onset and this decrease shifted to cue onset during

597 aversive conditioning. An important goal of future studies will be to use GRAB_{DA}
598 sensors to determine whether the same or different types of DANs are involved
599 in appetitive vs. aversive learning.

600

601 Our experiments in freely behaving male mice provide new perspectives with
602 respect to DA dynamics during sexual behaviors. Contrary to traditional views,
603 GRAB_{DA} sensors expressed in the NAc revealed striking time-locked DA
604 elevation immediately prior to and peak at the onset of various distinct sexual
605 behaviors, consistent with a model where DA encodes behavioral motivation,
606 anticipation, or arousal. These rapid changes in DA levels are in contrast with
607 previous dialysis studies showing that DA levels in the NAc slowly increase
608 during sexual behaviors, a difference that likely relates to the slow readout
609 associated with dialysis-based methods. The targeted expression of GRAB_{DA}
610 sensors could therefore provide a critical window into the coding strategy of DA
611 release in complex behaviors. Moreover, because GRAB_{DA} sensors readily
612 discriminate between DA and NE, they may be useful in studying cortical and
613 subcortical regions in which dopaminergic and adrenergic inputs are
614 intertwined.

615

616 Given that the crystal structure of the D₂R was recently solved (Wang et al.,
617 2018), future efforts can use this structural information to further tune the affinity,
618 enhance the selectivity, and increase the signal-to-noise ratio in the next-
619 generation of GRAB_{DA} sensors. Moreover, by adding a red fluorescent protein,
620 GRAB_{DA} sensors can be readily transformed into ratiometric indicators, which
621 could prove useful for more quantitative measurements of DA release across
622 different experiments and preparations. Finally, a GPCR-based strategy was
623 recently used to develop a genetically-encoded sensor (GACH) with high
624 sensitivity and high selectivity for acetylcholine (ACh) (Miao Jing et al., 2018).
625 Although the GACH sensor differs from the GRAB_{DA} sensors described here in
626 that is based on the muscarinic Gq-coupled GPCR receptor M₃R and an ICL3
627 loop derived from a Gs-coupled beta adrenergic receptor (Levitzki, 1988;
628 Rasmussen et al., 2011), a feature common to this sensor is that the
629 conformational changes in a GPCR induced by ligand binding are successfully
630 harnessed and converted into a sizable increase in cpEGFP fluorescence. Given
631 the diverse ligand-specificity of different GPCRs, a future goal will be to explore
632 whether this principle can be expanded even further in order to develop sensors
633 for the entire range of neurotransmitters and neuromodulators.

634

635 **Methods**

636 **Animals**

637

638 Wild-type Sprague-Dawley rat pups (P0) were used to prepare cultured cortical
639 neurons. Wild-type C57BL/6 and TH-Cre mice (B6.FVB(Cg)-Tg(Th-
640 cre)F1172Gsat/Mmucd obtained from MMRRC) were used to prepare the acute
641 brain slices and *in vivo* experiments. All animals were maintained in the animal
642 facilities and were family- or pair-housed in a temperature-controlled room with
643 a 12-h/12-h light/dark cycle. All procedures for animal surgery and maintenance
644 were performed using protocols that were approved by the Animal Care & Use
645 Committees at Peking University, Chinese Academy of Sciences (CAS), New
646 York University, University of California, San Francisco, and US National
647 Institutes of Health, and were performed in accordance with the guidelines
648 established by US National Institutes of Health guidelines.

649

650 To generate transgenic zebrafish, plasmids containing pTol2-elval3:GRAB_{DA1m}
651 (25 ng/ μ L) and Tol2 mRNA (25 ng/ μ L) were co-injected into fertilized eggs, and
652 founders were screened three months later. Transgenic zebrafish adults and
653 larvae were maintained at 28 °C on a 14-h/10-h light/dark cycle.

654

655 To generate transgenic flies, the coding sequence of GRAB_{DA1m} was integrated
656 into the pUAST vector using Gibson Assembly (Gibson et al., 2009), which was
657 then used in P-element-mediated random insertion. Transgenic *Drosophila*
658 lines carrying GRAB_{DA1m} on the chromosomes 2 and 3 with the strongest
659 expression level after crossing with TH-GAL4 were used. The coding sequence
660 of GRAB_{DA1m-mut} was incorporated into pJFRC28 (Pfeiffer et al., 2012)
661 (Addgene plasmid #36431) using Gibson Assembly, and this plasmid was used
662 to generate transgenic flies using PhiC31-mediated site-directed integration
663 into attp40. The embryo injections were performed at Core Facility of
664 *Drosophila* Resource and Technology, Shanghai Institute of Biochemistry and
665 Cell Biology, CAS. Transgenic flies were raised on conventional corn meal at
666 25°C, with ~70% humidity, under 12:12-h light-dark cycle.

667

668 The following *Drosophila* lines used in this study:

669 TH-GAL4, a gift and unpublished line generated by appending 2A-GAL4 to the
670 last exon of TH, from Yi Rao, Peking University. C305a-GAL4 and 30y-GAL4,

671 also gifts from Yi Rao. $DTH^{FS+/-}ple^2/TM6B$ (Cichewicz et al., 2017), a gift from
672 Jay Hirsh, University of Virginia. UAS-DAT-RNAi (TH01470.N), from Tsinghua
673 Fly center, Tsinghua University. UAS-jRCaMP1a (Bloomington #63792), a gift
674 from Chuan Zhou, Institute of Zoology, Chinese Academy of Sciences.

675 The following genotypes were used in the following figures:

676 Fig. 4A-C

677 UAS-GRAB_{DA1m}/cyo; TH-GAL4 (DANs)/TM6B

678 UAS-GRAB_{DA1m-mut}/+; TH-GAL4/+

679 c305a-GAL4 (α' and β' Kenyon cells)/UAS-GRAB_{DA1m} ; $DTH^{FS+/-}ple^2/+$ (WT
680 group)

681 c305a-GAL4/UAS-GRAB_{DA1m} ; $DTH^{FS+/-}ple^2$ (TH-deficient group)

682 Fig. 4D-K

683 UAS-GRAB_{DA1m}/cyo; TH-GAL4/TM6B

684 UAS-GRAB_{DA1m-mut}/+; TH-GAL4/+

685 Fig. 4L-O

686 UAS-GRAB_{DA1m}/cyo; TH-GAL4/TM6B

687 UAS-GRAB_{DA1m}/+; TH-GAL4/UAS-DAT-RNAi

688 Fig. S5

689 TH-GAL4/ UAS-jRCaMP1a

690 UAS-GRAB_{DA1m}/+; TH-GAL4/UAS-jRCaMP1a

691 30y-GAL4/ UAS-jRCaMP1a

692 UAS-GRAB_{DA1m}/+; 30y-GAL4/UAS-jRCaMP1a

693

694 **Molecular biology**

695

696 Plasmids were generated using Gibson Assembly. DNA fragments were
697 generated using PCR amplification with primers (Thermo Fisher Scientific) with
698 30-bp overlap. The fragments were assembled using T5-exonuclease (New
699 England Biolabs), Phusion DNA polymerase (Thermo Fisher Scientific), and
700 Taq ligase (iCloning). All sequences were verified using Sanger sequencing
701 (Sequencing platform in the School of Life Sciences of Peking University). DNA

702 encoding the various DA receptor subtypes (D₁R-D₅R) was generated using
703 PCR amplification of the full-length human GPCR cDNAs (hORFeome
704 database 8.1). For characterization in HEK293T cells, the GRAB_{DA} constructs
705 were cloned into the pDisplay vector (Invitrogen), with an IgK leader sequence
706 inserted upstream of the coding region. The IRES-mCherry gene was attached
707 downstream of GRAB_{DA} and was used as a reference of membrane marker to
708 calibrate of the signal intensity. Site-directed mutagenesis of the N- and C-
709 terminal linker sequences in cpEGFP was performed using primers containing
710 randomized NNB codons (48 codons in total, encoding the 20 possible amino
711 acids; Thermo Fisher Scientific). Site-directed mutagenesis of the D₂R gene
712 was performed using primers containing the target sites. For the
713 characterization in cultured neurons, the GRAB_{DA} constructs were cloned into
714 the pAAV vector under the TRE promoter or the human synapsin promoter. The
715 marker constructs RFP(mScarlet)-CAAX, EGFP-CAAX, KDELR1-EGFP,
716 PSD95-mScarlet and synaptophysin-mScarlet were cloned into pEGFP-N3
717 vector.

718

719 **Expression of GRAB_{DA} in cultured cells and *in vivo***

720

721 HEK293T cells were cultured in DMEM supplemented with 10% (v/v) FBS
722 (Gibco) and 1% penicillin-streptomycin (Gibco) at 37°C in 5% CO₂. The cells
723 were plated on 12-mm glass coverslips in 24-well plates and grown to ~50%
724 confluence for transfection. Transfection was performed by incubating the
725 HEK293T cells with a mixture containing 1 µg of DNA and 3 µg of PEI for 6 h.
726 Imaging was performed 24-48 h after transfection.

727

728 Rat cortical neurons were prepared from postnatal 0-day old (P0) Sprague-
729 Dawley rat pups as previously described (Zhang et al., 2009). In brief, the
730 cortical neurons were dissociated from the dissected rat brains in 0.25%
731 Trypsin-EDTA (Gibco), and plated on 12-mm glass coverslips coated with poly-
732 D-lysine (Sigma-Aldrich) in neurobasal medium containing 2% B-27
733 supplement, 1% GlutaMax, and 1% penicillin-streptomycin (Gibco). The cells
734 were transfected 7-9 days later using the calcium phosphate transfection
735 method. Imaging was performed 48-72 h after transfection.

736

737 For *in vivo* expression, Wild-type C57/BL6 mice with the age of P42-60 were
738 first anesthetized by 2,2,2-Tribromoethanol (Avetin, 500 mg/kg) through

739 intraperitoneal injection, or by isoflurane (RWD Life Science), and then placed
740 in a stereotaxic frame to inject AAVs of GRAB_{DA} sensors into NAc with a
741 microsyringe pump (Nanoliter 2000 Injector, WPI), or a microinjection pipette
742 injector (Nanoject II, Drummond Scientific). The coordination of NAc was set as
743 AP: -1.40 mm from Bregma, ML: 1.00 mm from the midline, DV: 3.90 mm from
744 the brain surface. The injection was made unilateral with ~300-500 nL per
745 animal. In dual-color optical recordings experiments, the AAVs of hsyn-
746 GRAB_{DA1m} and hsyn-tdTomato were injected in the dorsal striatum (AP = -
747 0.5mm, ML = ±2.5mm from bregma, and DV = -2.2mm from the brain surface),
748 and AAV of Ef1a-DIO-C1V1-YFP was injected in the substantia nigra pars
749 compacta (SNc) (AP = -3.1mm, ML = ±1.5mm from bregma, and DV = -4.0mm
750 from the brain surface) in TH-Cre mice.

751

752 **Fluorescence imaging of HEK293T cells and cultured neurons**

753

754 GRAB_{DA}-expressing HEK293T cells and cultured neurons were imaged using
755 an inverted Ti-E A1 confocal microscope (Nikon) and the Opera Phenix high
756 content screening system (PerkinElmer). The Nikon confocal microscope was
757 equipped with a 40×/1.35 NA oil immersion objective, a 488-nm laser and a
758 561-nm laser. During imaging, the HEK293T cells and cultured neurons were
759 bathed or perfused in a chamber with Tyrode's solution containing (in mM): 150
760 NaCl, 4 KCl, 2 MgCl₂, 2 CaCl₂, 10 HEPES and 10 glucose (pH 7.4). Solutions
761 containing the drug/compound of interest (e.g., DA, Halo, 5-HT, histamine, NE,
762 or ACh) were delivered via a custom-made perfusion system or via bath
763 application. The chamber was fully cleaned with Tyrode's solution and 75%
764 ethanol between experiments. The GFP signals (e.g., the GRAB_{DA} sensors, the
765 iGluSnFR or EGFP) were recorded using a 525/50 nm emission filter, and the
766 RFP signals were collected using a 595/50 nm emission filter. The
767 photostabilities of GRAB_{DA1m}, GRAB_{DA1h}, EGFP, and iGluSnFR were measured
768 using 350-μW 488-nm laser illumination. Photobleaching was applied to the
769 entire sensor-expressing HEK293T cell. The Opera Phenix high content
770 screening system was equipped with a 60×/ 1.15 NA water immersion objective,
771 a 488-nm laser, and a 561-m laser. The GRAB_{DA} signals were collected using
772 a 525/50 nm emission filter, and the mCherry signals were collected using a
773 600/30 nm emission filter. Where indicated, the culture medium was replaced
774 with 100 μl of Tyrode's solution containing various concentrations of the
775 indicated drug/compound. The fluorescence intensities of the GRAB_{DA} sensors
776 were calibrated using mCherry as the reference.

777

778 **Fluorescence imaging of GRAB_{DA} in brain slices**

779

780 Two weeks after the virus injection, the animals were anesthetized with Avetin
781 and then decapitated. The brains were removed immediately and placed
782 directly in cold slicing buffer containing (in mM): 110 choline-Cl, 2.5 KCl, 1.25
783 NaH₂PO₄, 25 NaHCO₃, 7 MgCl₂, 25 glucose, and 2 CaCl₂. The brains were then
784 sectioned into 200- μ m thick slices using a VT1200 vibratome (Leica, Germany),
785 and the sections were transferred into the oxygenated Ringer's buffer
786 containing (in mM): 125 NaCl, 2.5 KCl, 1.25 NaH₂PO₄, 25 NaHCO₃, 1.3 MgCl₂,
787 25 glucose, and 2 CaCl₂; the slices were then allowed to recover in 34 °C for at
788 least 40 minutes. For fluorescence imaging, the slices were transferred to an
789 imaging chamber in an Olympus FV1000MPE two-photon microscope
790 equipped with a 40 \times /0.80 NA water-immersion objective and a mode-locked
791 Mai Tai Ti:Sapphire laser (Spectra-Physics) tuned to 920 nm for the excitation
792 of GRAB_{DA} sensors and a 495~540 nm filter for signal collection. For electrical
793 stimulation, a concentric electrode (model #CBAEC75, FHC) was positioned
794 near the NAc core under the fluorescence guidance, and the imaging and
795 stimulation were synchronized using an Arduino board with custom programs.
796 The stimulation voltage was set at 5-6 V, and the duration of each stimulation
797 was set at 2 ms.

798

799 For immunostaining of brain sections, GRAB_{DA}-expressing mice were
800 anesthetized with Avetin, and the heart was perfused with 0.9% NaCl followed
801 with 4% paraformaldehyde (PFA). The brain was then removed and placed in
802 4% PFA for 4 hours, then cryoprotected in 30% (w/v) sucrose for 24 hours. The
803 brain was embedded into tissue-freezing medium, and 50- μ m-thick coronal
804 sections were cut using a Leica CM1900 cryostat (Leica, Germany). To label
805 dopaminergic terminals and GRAB_{DA} in the NAc, tissue sections were rinsed
806 and then immunostained with rabbit anti-TH antibody (1:100, Millipore, #ab152)
807 and chicken anti-GFP antibody (1:500, Abcam, #ab13970), followed by an
808 Alexa-555-conjugated goat-anti-rabbit and Alexa-488-conjugated goat-anti-
809 chicken secondary antibodies. The immunostained tissue sections were
810 imaged using the same Nikon confocal microscope in cell imaging.

811

812 **Fluorescence imaging of transgenic flies**

813

814 Adult *Drosophila* (within 3 weeks of eclosion) were used for imaging

815 experiments. The mounting and dissection protocols were as previously
816 described (Liang et al., 2013). In brief, a section of rectangular cuticle between
817 the eyes was removed to expose the brain, which was then bathed in saline,
818 so called adult hemolymph-like solution (AHLS). The same Olympus two-
819 photon microscope used for brain slices imaging was also used here. For
820 GRAB_{DA} sensors imaging, 920-nm excitation laser and 495~540-nm filter were
821 used. For jRCaMP1a, 1000-nm excitation laser and 575~630-nm filter were
822 used. For olfactory stimulation, the odorant isoamyl acetate (Sigma-Aldrich; Cat.
823 #306967) was firstly diluted 200-fold in mineral oil in a bottle; this dilution was
824 subsequently diluted 5-fold in air, which was then delivered to the fly's antenna
825 at a rate of 1000 ml/min. Compounds such as Halo and cocaine were added
826 directly to the AHLS to their final concentration, and the following experiments
827 were performed 10 min after compound application. For electrical stimulation,
828 a glass electrode (resistance ~0.2 MΩ) was placed in the region of the DANs in
829 the MB and the stimulation voltage was set at 20~80 V. Arduino was used to
830 synchronized stimulation delivery and imaging with custom code. The sampling
831 rates during olfactory stimulation and electrical stimulation was 2.7 Hz and 12
832 Hz, respectively.

833

834 **Fluorescence imaging and chemogenetics in zebrafish**

835

836 All experiments were performed on 5 days-post-fertilization (5 dpf) larvae in 10%
837 Hank's solution containing (in mM): 140 NaCl, 5.4 KCl, 0.25 Na₂HPO₄, 0.44
838 KH₂PO₄, 1.3 CaCl₂, 1.0 MgSO₄, and 4.2 NaHCO₃ (pH 7.2). Imaging of Tg
839 (elval3:GRAB_{DA1m}/DAT:TRPV1-TagRFP) larvae at 5 dpf was performed with an
840 inverted confocal microscope (Olympus FV3000, Japan) using a 30X oil-
841 immersion objective (1.05 N.A., morphology imaging) or an upright confocal
842 microscope (Olympus FV1000, Japan) using 40X water-immersion objective
843 (0.8 NA, time-lapse imaging). After the larvae were paralyzed with α-
844 bungarotoxin (100 μg/ml, Sigma), they were mounted dorsal side up in 1.5%
845 low melting-point agarose (Sigma) and then immersed in an extracellular
846 solution consisting of (in mM): 134 NaCl, 2.9 KCl, 4 CaCl₂, 10 HEPES and 10
847 glucose (290 mOsmol/L, pH 7.8). For imaging the morphology, images were
848 acquired with a field of view consisting of 1,024 pixels × 1,024 pixels with spatial
849 resolution of 0.414 × 0.414 × 1 μm³ (x × y × z). For bath application of
850 compounds, dopamine (100 μM in 1 mM ascorbic acid solution, Sigma) was
851 added by pipette at ~ 4 min and haloperidol (50 μM in DMSO, Tocris) at ~12
852 min. These images were acquired with a view field of 640 × 640 pixels with
853 spatial resolution of 0.497 × 0.497 μm² (x × y) at ~1.5 Hz. For functional imaging,

854 small anterior dissections initiated in ventricles were made, after which a glass
855 pipette containing the TRPV1 agonist capsaicin (50 μ M in absolute ethanol,
856 Tocris) was advanced through the incision and placed near the cell bodies of
857 the DANs. To activate the DANs, 5 pulses of puffs (9-10 psi, 100-ms) were
858 delivered with 1 min interval. The larvae were bath in Halo (50 μ M in DMSO,
859 Tocris) for 10 min before imaging. These images were acquired with a field of
860 view consisting of 800 \times 800 pixels with spatial resolution of 0.397 \times 0.397 μ m²
861 (x \times y) at \sim 1 Hz.

862

863 **Fiber Photometry recording in freely moving mice**

864

865 In all-optic experiments in Fig. 6, optical fiber probes (105 μ m core /125 μ m
866 cladding) were implanted in the dorsal striatum and in SNc 4 weeks after the
867 virus injection. Fiber photometry recording in the dorsal striatum was performed
868 using a 50- μ W 470-nm LED, and C1V1 in the SNc was stimulated using a 9.9-
869 mW 561-nm laser. The measured emission spectra of GRAB_{DA1m} and tdTomato
870 were fitted using a linear unmixing algorithm
871 <https://www.niehs.nih.gov/research/atniehs/labs/In/pi/iv/tools/index.cfm>. The
872 coefficients of GRAB_{DA1m} and tdTomato generated by the unmixing algorithm
873 were used to represent the fluorescence intensities of GRAB_{DA1m} and tdTomato,
874 respectively. To evoke C1V1-mediated DA release in the dorsal lateral striatum,
875 pulse trains (10-ms pulses at 10 Hz for 1 s) were delivered to the SNc using a
876 9.9-mW, 561-nm laser. In other experiments in Fig. 7 and 8, an optic fiber
877 (Thorlabs, FT200UMT, FT400UMT or BFH48-400) was attached to the
878 implanted ferrule (Thorlabs, SF440-10) via a ceramic sleeve. A 400-Hz
879 sinusoidal blue LED light (30 μ W) (LED light: M470F1; LED driver: LEDD1B;
880 both from Thorlabs) was bandpass filtered (passing band: 472 \pm 15 nm,
881 Semrock, FF02-472/30-25 in Fig.8 or 460-490nm in Fig.7) and delivered to the
882 brain to excite GRAB_{DA}. The emission light then traveled through the same optic
883 fiber, was bandpass filtered (passing band: 534 \pm 25 nm, Semrock, FF01-
884 535/50 in Fig.8 or 500-550nm in Fig.7), detected by a Femtowatt Silicon
885 Photoreceiver (Newport, 2151) and recorded using a real-time processor (RZ5,
886 TDT). The envelope of the 400-Hz signals that reflects the intensity of the
887 fluorescence signals was extracted in real-time using a custom TDT program.

888

889 **Behaviors**

890

891 For the auditory conditioning task, mice were recovered for >3 days after
892 surgery, and then water-restricted until reaching 85-90% of its original body
893 weight and then prepared for behavior training. In the first Pavlovian task, the
894 mice were trained on two frequency modulated pure tone auditory cues of 500
895 ms in duration, centered around 2.5 kHz and 11 kHz. For each mouse, one of
896 the two tones was pseudo-randomly assigned to be the reward-predictive tone.
897 Reward (water sweetened with 10% sucrose) was delivered through a water
898 spout in front of the mouth following the reward-predictive cue with a variable
899 500-1500 ms delay. Rewarded and unrewarded trials were randomly
900 interleaved with a variable inter-trial interval of 8-20 s. Mice experienced 200
901 trials (~100 rewards) per day in sessions lasting ~45 min.

902

903 In the subsequent Pavlovian conditioning task, the mice were trained on an
904 auditory conditioning task, in which three pairs of auditory cues → outcomes
905 pairs (or CS-US pairs; 8 kHz pure tone → 9 μ l water; white noise → brief air
906 puff to the face; and 2 kHz pure tone → no response) were delivered at
907 random with a 10 -20 s randomized inter-trial interval. The duration and intensity
908 of each auditory cue was 1 s and 70dB, respectively. The respective outcomes
909 was delivered 1 s after the end of each auditory cue. The behavioral setup
910 consisted of a custom-built apparatus allowing head fixation of the mouse's
911 head to a Styrofoam rod (diameter: 15 cm). Rotation of the Styrofoam rod,
912 which corresponds to the animal's running speed, was detected using an optical
913 rotatory encoder. Licking behavior was detected when the mouse's tongue
914 contacted the water delivery tube. Each lick signal was processed using an
915 Arduino UNO board with custom code and sent digitally to the training program
916 (written in MATLAB) via a serial port. Water delivery was precisely controlled
917 using a stepping motor pump, and the air puff (15 psi, 25-ms duration) was
918 controlled using a solenoid valve. Timing of the pump and valve was controlled
919 using the same Arduino UNO board used for lick detection, which also provided
920 synchronization between the training program and the data acquisition system
921 (RZ2 processor, Tucker-Davis Technologies). During first two days of each
922 training session, the outcomes were delivered without the prediction cues.

923

924 The sexual behaviors are defined following conventions in previous literature
925 (Hull and Rodriguez-Manzo, 2009). In details, sniffing female was defined as
926 the male's nose coming in close proximity to the female's facial, body, and/or
927 urogenital areas. "Mount" was defined as when the male posed his forelegs
928 over the female's back and with his hindfeet on the ground accompanying
929 shallow pelvic thrusts. The mounting onset was defined as the moment at which

930 the male tried to clasp female back. “Intromission” was defined as a deep
931 rhythmic thrust following mounting. The onset of intromission was defined as
932 the time at which the male performed the first deep thrusting toward the female
933 with vaginal penetration. “Penile grooming” was defined when a male animal
934 repeated grooming for his urogenital area after intromission and ejaculation.
935 Ejaculation is detected when the male stopped thrusting and freeze for
936 seconds. The putative ejaculation event was confirmed by the presence of
937 vaginal copulatory plug.

938

939 **Data analysis**

940

941 For imaging experiments in HEK293T cells, neurons, acute brain slices and
942 transgenic flies, images were first analyzed using Image J software (National
943 Institutes of Health), and then analyzed using Origin 9.1 (OriginLab) and
944 MATLAB (MathWorks) with custom-written scripts. The data in acute brain slices
945 and flies were first binned by 2x and averaged to generate representative traces.

946

947 For fiber photometry data, the signal baseline was first obtained by the MATLAB
948 function “msbackadj” with a moving window of 25% of the total recording
949 duration in Fig.8, or by subtracting 2nd order exponential fitted data from the raw
950 data after 10.17 Hz binning in Fig. 7. The fluorescence responses were
951 indicated by $\Delta F/F_0$ in Fig.8, which was calculated as $(F_{\text{raw}} - F_{\text{baseline}})/F_{\text{baseline}}$, or
952 by Z score in Fig.7. To analyze event-evoked changes in DA release, we
953 aligned each trial to the onset or offset of the behavior, and calculated the peri-
954 stimulus time histogram (PSTH). To compare PSTH changes during different
955 phases of the training, we used data from the 2nd day as naive, the 5-10th day
956 as trained and >10th day as well-trained, and normalized the PSTH of each
957 animal by water-evoked response during early training. The peak response
958 during a behavior was calculated as the maximum $\Delta F/F_0$ during the behavior
959 minus the average $\Delta F/F_0$ in the duration-matched period 2s prior to the behavior
960 onset in Fig.8. The response to the CS was defined as the peak of the
961 normalized PSTH between the CS onset and the US onset, and the response
962 to US was calculated similarly using data from the US onset to data collected 2
963 s after the US onset in Fig.7.

964

965 Except where indicated otherwise, group differences were analyzed using the
966 Student’s *t*-test, test, sign-rank test, One-Way ANOVA or post-hoc Tukey’s test.

967 Except where indicated otherwise, all summary data presented as the mean \pm
968 SEM.

969

970 **Acknowledgements**

971 This work was supported by the National Basic Research Program of China
972 (973 Program; grant 2015CB856402), the General Program of National Natural
973 Science Foundation of China (project 31671118 and project 31371442), an NIH
974 brain initiative grant NS103558, and the Junior Thousand Talents Program of
975 China to Y.Li and to S.Zhang. Additional support was provided by the Ministry
976 of Science and Technology of the People's Republic of China
977 (2017YFA0505703) to M.Xu. We thank Y. Rao for sharing the 2-photon
978 microscope and X. Lei for the platform support of Opera Phenix high content
979 screening system at PKU-CLS. We thank the sequencing platform in the School
980 of Life Sciences of Peking University. We thank R. Mooney, Y. Huan and L. Luo
981 for valuable feedback of the manuscript.

982

983 **Author Contributions**

984 Y.L. conceived and supervised the project. F.S., M.J., and J.Z. performed
985 experiments related to sensor development, optimization and characterization
986 in culture HEK cells, culture neurons, brain slices and transgenic flies, with the
987 initial work from YC. L. and J. F., and help from Z.Y.. F.L. and J.D. designed
988 and performed experiments on transgenic fish. J.Z., Y.G., T.Y., W.P., S.O.,
989 L.W., S.Z., D.L., M.X., A.K., and G.C. designed and performed experiments in
990 behaving mice. All authors contributed to data interpretation and data analysis.
991 Y.L. wrote the manuscript with input from F.S., J.Z., M.J., D.L., S.O., M.X. and
992 help from other authors.

993

994 **References**

- 995 Abercrombie, E.D., Keefe, K.A., DiFrischia, D.S., and Zigmond, M.J. (1989). Differential effect of stress on
996 in vivo dopamine release in striatum, nucleus accumbens, and medial frontal cortex. *Journal of*
997 *neurochemistry* 52, 1655-1658.
- 998 Aso, Y., and Rubin, G.M. (2016). Dopaminergic neurons write and update memories with cell-type-
999 specific rules. *Elife* 5.
- 1000 Aso, Y., Siwanowicz, I., Bracker, L., Ito, K., Kitamoto, T., and Tanimoto, H. (2010). Specific dopaminergic
1001 neurons for the formation of labile aversive memory. *Current biology : CB* 20, 1445-1451.
- 1002 Bainton, R.J., Tsai, L.T., Singh, C.M., Moore, M.S., Neckameyer, W.S., and Heberlein, U. (2000). Dopamine
1003 modulates acute responses to cocaine, nicotine and ethanol in *Drosophila*. *Curr Biol* 10, 187-194.

- 1004 Balleine, B.W., Delgado, M.R., and Hikosaka, O. (2007). The role of the dorsal striatum in reward and
1005 decision-making. *The Journal of neuroscience : the official journal of the Society for Neuroscience* 27,
1006 8161-8165.
- 1007 Barnea, G., Strapps, W., Herrada, G., Berman, Y., Ong, J., Kloss, B., Axel, R., and Lee, K.J. (2008). The
1008 genetic design of signaling cascades to record receptor activation. *Proceedings of the National Academy*
1009 *of Sciences* 105, 64-69.
- 1010 Bayer, H.M., and Glimcher, P.W. (2005). Midbrain dopamine neurons encode a quantitative reward
1011 prediction error signal. *Neuron* 47, 129-141.
- 1012 Beaulieu, J.M., and Gainetdinov, R.R. (2011). The physiology, signaling, and pharmacology of dopamine
1013 receptors. *Pharmacol Rev* 63, 182-217.
- 1014 Berridge, K.C., and Robinson, T.E. (1998). What is the role of dopamine in reward: Hedonic impact,
1015 reward learning, or incentive salience? , pp. 309-369.
- 1016 Brooks, A.M., and Berns, G.S. (2013). Aversive stimuli and loss in the mesocorticolimbic dopamine
1017 system, pp. 281-286.
- 1018 Burke, C.J., Huetteroth, W., Oswald, D., Perisse, E., Krashes, M.J., Das, G., Gohl, D., Silies, M., Certel, S.,
1019 and Waddell, S. (2012). Layered reward signalling through octopamine and dopamine in *Drosophila*.
1020 *Nature* 492, 433-437.
- 1021 Burns, D.L. (1988). Subunit structure and enzymic activity of pertussis toxin. *Microbiol Sci* 5, 285-287.
- 1022 Chien, E.Y.T., Liu, W., Zhao, Q., Katritch, V., Han, G.W., Hanson, M.A., Shi, L., Newman, A.H., Javitch, J.A.,
1023 and Cherezov, V. (2010a). Structure of the human dopamine D3 receptor in complex with a D2/D3
1024 selective antagonist. *Science* 330, 1091-1095.
- 1025 Chien, E.Y.T., Liu, W., Zhao, Q., Katritch, V., Han, G.W., Hanson, M.A., Shi, L., Newman, A.H., Javitch, J.A.,
1026 Cherezov, V., *et al.* (2010b). Structure of the human dopamine D3 receptor in complex with a D2/D3
1027 selective antagonist. *Science (New York, NY)* 330, 1091-1095.
- 1028 Cichewicz, K., Garren, E., Adiele, C., Aso, Y., Wang, Z., Wu, M., Birman, S., Rubin, G., and Hirsh, J. (2017).
1029 A new brain dopamine - deficient *Drosophila* and its pharmacological and genetic rescue. *Genes, Brain*
1030 *and Behavior* 16, 394-403.
- 1031 Cognigni, P., Felsenberg, J., and Waddell, S. (2017). Do the right thing: neural network mechanisms of
1032 memory formation, expression and update in *Drosophila*. *Curr Opin Neurobiol* 49, 51-58.
- 1033 Cohn, R., Morantte, I., and Ruta, V. (2015). Coordinated and compartmentalized neuromodulation
1034 shapes sensory processing in *Drosophila*. *Cell* 163, 1742-1755.
- 1035 Cook Jr, E.H., Stein, M.A., Krasowski, M.D., Cox, N.J., Olkon, D.M., Kieffer, J.E., and Leventhal, B.L. (1995).
1036 Association of attention-deficit disorder and the dopamine transporter gene. *American journal of*
1037 *human genetics* 56, 993.
- 1038 Da Silva, J.A., Tecuapetla, F., Paixão, V., and Costa, R.M. (2018). Dopamine neuron activity before action
1039 initiation gates and invigorates future movements. *Nature* 554, 244-248.
- 1040 Damsma, G., Pfaus, J.G., Wenkstern, D., Phillips, A.G., and Fibiger, H.C. (1992). Sexual Behavior Increases
1041 Dopamine Transmission in the Nucleus Accumbens and Striatum of Male Rats: Comparison With
1042 Novelty and Locomotion. *Behavioral Neuroscience* 106, 181-191.
- 1043 Daw, N.D., and Tobler, P.N. (2013). Value Learning through Reinforcement: The Basics of Dopamine and
1044 Reinforcement Learning. In, pp. 283-298.
- 1045 Di Chiara, G., and Imperato, A. (1988). Drugs abused by humans preferentially increase synaptic
1046 dopamine concentrations in the mesolimbic system of freely moving rats. *Proc Natl Acad Sci U S A* 85,
1047 5274-5278.

- 1048 Fox, M.E., and Wightman, R.M. (2016). Contrasting Regulation of Catecholamine Neurotransmission in
1049 the Behaving Brain: Pharmacological Insights from an Electrochemical Perspective. *Pharmacological*
1050 *reviews* *69*, 12-32.
- 1051 Gibson, D.G., Young, L., Chuang, R.Y., Venter, J.C., Rd, H.C., and Smith, H.O. (2009). Enzymatic assembly
1052 of DNA molecules up to several hundred kilobases. *Nature Methods* *6*, 343.
- 1053 Giros, B., Jaber, M., Jones, S.R., Wightman, R.M., and Caron, M.G. (1996). Hyperlocomotion and
1054 indifference to cocaine and amphetamine in mice lacking the dopamine transporter. *Nature* *379*, 606-
1055 612.
- 1056 Glimcher, P.W. (2011). Understanding dopamine and reinforcement learning: The dopamine reward
1057 prediction error hypothesis. *Proceedings of the National Academy of Sciences* *108*, 15647-15654.
- 1058 Gonzales, R.A., Job, M.O., and Doyon, W.M. (2004). The role of mesolimbic dopamine in the
1059 development and maintenance of ethanol reinforcement, pp. 121-146.
- 1060 Graybiel, A.M., Aosaki, T., Flaherty, A.W., and Kimura, M. (1994). The basal ganglia and adaptive motor
1061 control. *Science* *265*, 1826-1831.
- 1062 Gunaydin, L.A., Grosenick, L., Finkelstein, J.C., Kauvar, I.V., Fenno, L.E., Adhikari, A., Lammel, S.,
1063 Mirzabekov, J.J., Airan, R.D., Zalocusky, K.A., *et al.* (2014). Natural neural projection dynamics underlying
1064 social behavior. *Cell* *157*, 1535-1551.
- 1065 Hancock, J.F., Cadwallader, K., Paterson, H., and Marshall, C.J. (1991). A CAAX or a CAAL motif and a
1066 second signal are sufficient for plasma membrane targeting of ras proteins. *The EMBO journal* *10*, 4033-
1067 4039.
- 1068 Heisenberg, M. (2003). Mushroom body memoir: from maps to models. *Nat Rev Neurosci* *4*, 266-275.
- 1069 Hernandez, L., and Hoebel, B.G. (1988). Food reward and cocaine increase extracellular dopamine in
1070 the nucleus accumbens as measured by microdialysis. *Life sciences* *42*, 1705-1712.
- 1071 Holroyd, C.B., and Coles, M.G.H. (2002). The neural basis of human error processing: reinforcement
1072 learning, dopamine, and the error-related negativity. *Psychol Rev* *109*, 679-709.
- 1073 Howe, M.W., and Dombeck, D.A. (2016). Rapid signalling in distinct dopaminergic axons during
1074 locomotion and reward. *Nature* *535*, 505-510.
- 1075 Howes, O.D., and Kapur, S. (2009). The dopamine hypothesis of schizophrenia: version III—the final
1076 common pathway. *Schizophrenia bulletin* *35*, 549-562.
- 1077 Hull, E.M., and Rodriguez-Manzo, G. (2009). Male sexual behavior. *Hormones, Brain and Behavior* *1*, 5-
1078 65.
- 1079 Hung, L.W., Neuner, S., Polepalli, J.S., Beier, K.T., Wright, M., Walsh, J.J., Lewis, E.M., Luo, L., Deisseroth,
1080 K., Dölen, G., *et al.* (2017). Gating of social reward by oxytocin in the ventral tegmental area. *Science*
1081 *357*, 1406-1411.
- 1082 Inagaki, H.K., de-Leon, S.B.-T., Wong, A.M., Jagadish, S., Ishimoto, H., Barnea, G., Kitamoto, T., Axel, R.,
1083 and Anderson, D.J. (2012). Visualizing neuromodulation in vivo: TANGO-mapping of dopamine signaling
1084 reveals appetite control of sugar sensing. *Cell* *148*, 583-595.
- 1085 Jaquins-Gerstl, A., and Michael, A.C. (2015). A review of the effects of FSCV and microdialysis
1086 measurements on dopamine release in the surrounding tissue. *Analyst* *140*, 3696-3708.
- 1087 Kim, M.W., Wang, W., Sanchez, M.I., Coukos, R., Von Zastrow, M., and Ting, A.Y. (2017). Time-gated
1088 detection of protein-protein interactions with transcriptional readout. *eLife* *6*.
- 1089 Kruse, A.C., Ring, A.M., Manglik, A., Hu, J., Hu, K., Eitel, K., HäBner, H., Pardon, E., Valant, C., and Sexton,
1090 P.M. (2013). Activation and allosteric modulation of a muscarinic acetylcholine receptor. *Nature* *504*,
1091 101-106.

- 1092 Kume, K., Kume, S., Park, S.K., Hirsh, J., and Jackson, F.R. (2005). Dopamine is a regulator of arousal in
1093 the fruit fly. *Journal of Neuroscience* *25*, 7377-7384.
- 1094 Lammel, S., Lim, B.K., and Malenka, R.C. (2014). Reward and aversion in a heterogeneous midbrain
1095 dopamine system. *Neuropharmacology* *76*, 351-359.
- 1096 Lanau, F., Zenner, M.-t., Civelli, O., and Hartman, D.S. (1997a). Epinephrine and Norepinephrine Act as
1097 Potent Agonists at the Recombinant Human Dopamine D4 Receptor.
- 1098 Lanau, F., Zenner, M.T., Civelli, O., and Hartman, D.S. (1997b). Epinephrine and norepinephrine act as
1099 potent agonists at the recombinant human dopamine D4 receptor. *Journal of Neurochemistry* *68*, 804-
1100 812.
- 1101 Lee, D., Creed, M., Jung, K., Stefanelli, T., Wendler, D.J., Oh, W.C., Mignocchi, N.L., Lüscher, C., and Kwon,
1102 H.-B. (2017). Temporally precise labeling and control of neuromodulatory circuits in the mammalian
1103 brain. *Nature methods* *14*, 495.
- 1104 Levitzki, A. (1988). From epinephrine to cyclic AMP. *Science* *241*, 800-806.
- 1105 Liang, L., Li, Y., Potter, C.J., Yizhar, O., Deisseroth, K., Tsien, R.W., and Luo, L. (2013). GABAergic projection
1106 neurons route selective olfactory inputs to specific higher-order neurons. *Neuron* *79*, 917-931.
- 1107 Liu, C., Placais, P.Y., Yamagata, N., Pfeiffer, B.D., Aso, Y., Friedrich, A.B., Siwanowicz, I., Rubin, G.M., Preat,
1108 T., and Tanimoto, H. (2012). A subset of dopamine neurons signals reward for odour memory in
1109 *Drosophila*. *Nature* *488*, 512-516.
- 1110 Lohse, M.J., Hein, P., Hoffmann, C., Nikolaev, V.O., Vilardaga, J.P., and Bunemann, M. (2008). Kinetics of
1111 G-protein-coupled receptor signals in intact cells. *Br J Pharmacol* *153 Suppl 1*, S125-132.
- 1112 Lotharius, J., and Brundin, P. (2002). Pathogenesis of Parkinson's disease: dopamine, vesicles and α -
1113 synuclein. *Nature Reviews Neuroscience* *3*, 932.
- 1114 Luttrell, L.M., and Lefkowitz, R.J. (2002). The role of beta-arrestins in the termination and transduction
1115 of G-protein-coupled receptor signals. *J Cell Sci* *115*, 455-465.
- 1116 Marvin, J.S., Borghuis, B.G., Tian, L., Cichon, J., Harnett, M.T., Akerboom, J., Gordus, A., Renninger, S.L.,
1117 Chen, T.-W., Bargmann, C.I., *et al.* (2013). An optimized fluorescent probe for visualizing glutamate
1118 neurotransmission. *Nature methods* *10*, 162-170.
- 1119 Mas, M., Fumero, B., and González-Mora, J. (1995). Voltammetric and microdialysis monitoring of brain
1120 monoamine neurotransmitter release during sociosexual interactions. *Behavioural Brain Research* *71*.
- 1121 Missale, C., Nash, S.R., Robinson, S.W., Jaber, M., and Caron, M.G. (1998). Dopamine receptors: from
1122 structure to function. *Physiol Rev* *78*, 189-225.
- 1123 Muller, A., Joseph, V., Slesinger, P.A., and Kleinfeld, D. (2014). Cell-based reporters reveal in vivo
1124 dynamics of dopamine and norepinephrine release in murine cortex. *Nature methods* *11*, 1245.
- 1125 Nair-Roberts, R.G., Chatelain-Badie, S.D., Benson, E., White-Cooper, H., Bolam, J.P., and Ungless, M.A.
1126 (2008). Stereological estimates of dopaminergic, GABAergic and glutamatergic neurons in the ventral
1127 tegmental area, substantia nigra and retrorubral field in the rat. *Neuroscience* *152*, 1024-1031.
- 1128 Neves, S.R., Ram, P.T., and Iyengar, R. (2002). G protein pathways, pp. 1636-1639.
- 1129 Nieoullon, A. (2002). Dopamine and the regulation of cognition and attention. *Progress in neurobiology*
1130 *67*, 53-83.
- 1131 Park, J., Kile, B.M., and Wightman, M.R. (2009). In vivo voltammetric monitoring of norepinephrine
1132 release in the rat ventral bed nucleus of the stria terminalis and anteroventral thalamic nucleus.
1133 *European Journal of Neuroscience* *30*, 2121-2133.
- 1134 Pfaus, J.G., Damsma, G., Nomikos, G.G., Wenkstern, D.G., Blaha, C.D., Phillips, A.G., and Fibiger, H.C.
1135 (1990a). Sexual behavior enhances central dopamine transmission in the male rat. *Brain Res* *530*, 345-

- 1136 348.
- 1137 Pfaus, J.G., Damsma, G., Nomikos, G.G., Wenkstern, D.G., Blaha, C.D., Phillips, A.G., and Fibiger, H.C.
1138 (1990b). Sexual behavior enhances central dopamine transmission in the male rat. *Brain Research* 530,
1139 345-348.
- 1140 Pfeiffer, B.D., Truman, J.W., and Rubin, G.M. (2012). Using translational enhancers to increase transgene
1141 expression in *Drosophila*. *Proceedings of the National Academy of Sciences* 109, 6626-6631.
- 1142 Pignatelli, M., and Bonci, A. (2015). Role of Dopamine Neurons in Reward and Aversion: A Synaptic
1143 Plasticity Perspective. *Neuron* 86, 1145-1157.
- 1144 Rasmussen, S.G.F., DeVree, B.T., Zou, Y., Kruse, A.C., Chung, K.Y., Kobilka, T.S., Thian, F.S., Chae, P.S.,
1145 Pardon, E., Calinski, D., *et al.* (2011). Crystal structure of the β 2 adrenergic receptor–Gs protein complex.
1146 *Nature* 477, 549-555.
- 1147 Ritz, M.C., Lamb, R., and Kuhar, M. (1987). Cocaine receptors on dopamine transporters are related to
1148 self-administration of cocaine. *Science* 237, 1219-1223.
- 1149 Robinson, D.L., Heien, M.L.a.V., and Wightman, R.M. (2002). Frequency of dopamine concentration
1150 transients increases in dorsal and ventral striatum of male rats during introduction of conspecifics. *The*
1151 *Journal of neuroscience : the official journal of the Society for Neuroscience* 22, 10477-10486.
- 1152 Robinson, D.L., Hermans, A., Seipel, A.T., and Wightman, R.M. (2008). Monitoring rapid chemical
1153 communication in the brain. *Chem Rev* 108, 2554-2584.
- 1154 Robinson, D.L., Phillips, P.E.M., Budygin, E.A., Trafton, B.J., Garris, P.A., and Wightman, R.M. (2001). Sub-
1155 second changes in accumbal dopamine during sexual behavior in male rats. *NeuroReport* 12, 2549-2552.
- 1156 Robinson, D.L., Venton, B.J., Heien, M.L., and Wightman, R.M. (2003). Detecting subsecond dopamine
1157 release with fast-scan cyclic voltammetry in vivo. *Clin Chem* 49, 1763-1773.
- 1158 Rodeberg, N.T., Sandberg, S.G., Johnson, J.A., Phillips, P.E., and Wightman, R.M. (2017). Hitchhiker's
1159 guide to voltammetry: acute and chronic electrodes for in vivo fast-scan cyclic voltammetry. *ACS*
1160 *chemical neuroscience* 8, 221-234.
- 1161 Sanchez-Soto, M., Bonifazi, A., Cai, N.S., Ellenberger, M.P., Newman, A.H., Ferre, S., and Yano, H. (2016).
1162 Evidence for Noncanonical Neurotransmitter Activation: Norepinephrine as a Dopamine D2-Like
1163 Receptor Agonist. *Molecular pharmacology* 89, 457-466.
- 1164 Schultz, W. (2006). Behavioral theories and the neurophysiology of reward. *Annual review of psychology*
1165 57, 87-115.
- 1166 Schultz, W. (2007). Behavioral dopamine signals, pp. 203-210.
- 1167 Schultz, W. (2016). Dopamine reward prediction-error signalling: a two-component response. *Nature*
1168 *Reviews Neuroscience* 17, 183.
- 1169 Schultz, W., Dayan, P., and Montague, P.R. (1997). A neural substrate of prediction and reward. *Science*
1170 275, 1593-1599.
- 1171 Schwaerzel, M., Monastirioti, M., Scholz, H., Friggi-Grelin, F., Birman, S., and Heisenberg, M. (2003).
1172 Dopamine and octopamine differentiate between aversive and appetitive olfactory memories in
1173 *Drosophila*. *J Neurosci* 23, 10495-10502.
- 1174 Shang, C.F., Li, X.Q., Yin, C., Liu, B., Wang, Y.F., Zhou, Z., and Du, J.L. (2015). Amperometric Monitoring
1175 of Sensory-Evoked Dopamine Release in Awake Larval Zebrafish. *J Neurosci* 35, 15291-15294.
- 1176 Sokoloff, P., Giros, B., Martres, M.-P., Bouthenet, M.-L., and Schwartz, J.-C. (1990). Molecular cloning and
1177 characterization of a novel dopamine receptor (D3) as a target for neuroleptics. *Nature* 347, 146-151.
- 1178 Sung, Y.M., Wilkins, A.D., Rodriguez, G.J., Wensel, T.G., and Lichtarge, O. (2016). Intramolecular allosteric
1179 communication in dopamine D2 receptor revealed by evolutionary amino acid covariation. *Proceedings*

1180 of the National Academy of Sciences of the United States of America *113*, 3539.
1181 Tidey, J.W., and Miczek, K.A. (1996). Social defeat stress selectively alters mesocorticolimbic dopamine
1182 release: an in vivo microdialysis study. *Brain Res* *721*, 140-149.
1183 Ungless, M.A., and Grace, A.A. (2012). Are you or aren't you? Challenges associated with physiologically
1184 identifying dopamine neurons. *Trends in neurosciences* *35*, 422-430.
1185 Ungless, M.A., Magill, P.J., and Bolam, J.P. (2004). Uniform inhibition of dopamine neurons in the ventral
1186 tegmental area by aversive stimuli. *Science* *303*, 2040-2042.
1187 van Erp, A.M., and Miczek, K.A. (2000). Aggressive behavior, increased accumbal dopamine, and
1188 decreased cortical serotonin in rats. *J Neurosci* *20*, 9320-9325.
1189 Vilardaga, J.-P., Bünemann, M., Krasel, C., Castro, M., and Lohse, M.J. (2003). Measurement of the
1190 millisecond activation switch of G protein-coupled receptors in living cells. *Nature biotechnology* *21*,
1191 807-812.
1192 Volkow, N.D., Wang, G.J., Fowler, J.S., Fischman, M., Foltin, R., Abumrad, N.N., Gatley, S.J., Logan, J.,
1193 Wong, C., Gifford, A., *et al.* (1999). Methylphenidate and cocaine have a similar in vivo potency to block
1194 dopamine transporters in the human brain. *Life Sciences* *65*.
1195 Wang, S., Che, T., Levit, A., Shoichet, B.K., Wacker, D., and Roth, B.L. (2018). Structure of the
1196 D₂ dopamine receptor bound to the atypical antipsychotic drug risperidone. *Nature* *2018*,
1197 1-24.
1198 Wang, S., Wacker, D., Levit, A., Che, T., Betz, R.M., Mccorvy, J.D., Venkatakrisnan, A.J., Huang, X.P., Dror,
1199 R.O., and Shoichet, B.K. (2017). D4 dopamine receptor high-resolution structures enable the discovery
1200 of selective agonists. *Science* *358*, 381-386.
1201 Wise, R.A. (2004). Dopamine, learning and motivation. *Nature reviews neuroscience* *5*, 483.
1202 Wisor, J.P., Nishino, S., Sora, I., Uhl, G.H., Mignot, E., and Edgar, D.M. (2001). Dopaminergic role in
1203 stimulant-induced wakefulness. *Journal of Neuroscience* *21*, 1787-1794.
1204 Yizhar, O., Fenno, L.E., Prigge, M., Schneider, F., Davidson, T.J., Ogshea, D.J., Sohal, V.S., Goshen, I.,
1205 Finkelstein, J., Paz, J.T., *et al.* (2011). Neocortical excitation/inhibition balance in information processing
1206 and social dysfunction. *Nature* *477*, 171-178.
1207 Zhang, Q., Li, Y., and Tsien, R.W. (2009). The Dynamic Control of Kiss-And-Run. *Science* *000858*, 1448-
1208 1453.
1209 Ziegler, N., Batz, J., Zabel, U., Lohse, M.J., and Hoffmann, C. (2011). FRET-based sensors for the human
1210 M1-, M3-, and M5-acetylcholine receptors. *Bioorg Med Chem* *19*, 1048-1054.

1211

1212 **Figure 1. Design, optimization and characterization of GRAB_{DA} sensors in**
1213 **cultured HEK293T cells.**

1214 (A-C) Schematic diagrams showing the strategy used to develop GRAB_{DA}
1215 sensors (top panels), and the corresponding performance of each variants in
1216 each optimization step (bottom panels).

1217 (A) Optimization of the cpEGFP insertion site within the third intracellular loop
1218 (ICL3) in D₂R. The $\Delta F/F_0$ of GRAB_{DA}-expressing cells in response to 100 μ M
1219 DA application is shown below. GRAB_{DA1m}, with the highest $\Delta F/F_0$ (~90%), was
1220 selected for further optimization. Each data point represents the average of 3-
1221 5 cells.

1222 (B) Optimization of the linkers between the D₂R and cpEGFP. Mutants were
1223 generated by changing each linker residue to 20 possible amino acids. The
1224 $\Delta F/F_0$ of the GRAB_{DA}-expressing cells relative to the brightness in response to
1225 100 μ M DA application is shown below. Each data point represents the average
1226 of 100-400 cells.

1227 (C) Affinity tuning. Either the T205M single mutation, or the C118A/S193N
1228 double mutations, were introduced into GRAB_{DA}, and the normalized dose-
1229 dependent fluorescence responses of various GRAB_{DA}-expressing cells in
1230 response to DA application are plotted below. Each data point represents
1231 average of 6 wells containing 100-400 cells per well.

1232 (D-E) Fluorescence changes in GRAB_{DA}-expressing cells in response to 100
1233 μ M DA followed by 10 μ M Halo. Peak $\Delta F/F_0$ values in response to DA are
1234 summarized in the right panel in (E) (GRAB_{DA1m}: $n = 18$ cells from 4 cultures
1235 (18/4); GRAB_{DA1m-mut}: $n = 15/3$; GRAB_{DA1h}: $n = 14/3$; GRAB_{DA1h-mut}: $n = 14/3$; p
1236 < 0.001 between DA1m and DA1m-mut; $p < 0.001$ between DA1h and DA1h-
1237 mut; $p = 0.42$ between DA1m and DA1h).

1238 (F) Schematic image showing the local perfusion system. A glass pipette (black
1239 dashed lines) filled with DA or Halo was positioned close to the GRAB_{DA}-
1240 expressing cells, and fluorescence was measured using confocal line-scanning
1241 (red line).

1242 (G) Left and middle: fluorescence changes in GRAB_{DA}-expressing cells in
1243 response to the local perfusion (on rate: 100 μ M DA in pipette with normal bath
1244 solution; off rate: 1 mM Halo in pipette with bath solution containing 10 μ M DA
1245 for GRAB_{DA1m} or 1 μ M DA for GRAB_{DA1h}). The traces are the average of 3
1246 different ROIs on the scanning line and are shaded with \pm SEM. Right: group
1247 data summarizing the response kinetics of GRAB_{DA}-expressing cells in
1248 response to DA (on) or Halo (off) ($n = 8$ /group; $p = 0.0093$ between on kinetics;
1249 $p < 0.001$ between off kinetics).

1250 (H) Normalized fluorescence changes in GRAB_{DA1m}- and GRAB_{DA1m-mut}-
1251 expressing cells in response to the application of indicated compounds at 1 μ M,
1252 including: DA, DA + Halo, DA + Etic, DA + SCH-23390 (SCH), norepinephrine
1253 (NE), 5-HT, histamine (His), glutamate (Glu), gamma-aminobutyric acid (GABA),
1254 adenosine (Ade), acetylcholine (ACh), tyramine (Tyr), octopamine (Oct),
1255 glycine (Gly), or L-DOPA (the first bar shows GRAB_{DA1m-mut}-expressing cells in
1256 response to DA; $n = 4$ wells per group with 200-400 cells per well; $p < 0.001$ for
1257 DA-induced responses between GRAB_{DA1m} and GRAB_{DA1m-mut}; $p = 0.99$ for
1258 GRAB_{DA1m} responses induced by DA comparing with DA+SCH; $p < 0.001$ for
1259 GRAB_{DA1m} responses induced by DA comparing with DA+Halo, DA+Etic, NE,
1260 5-HT, His, Glu, GABA, Ade, ACh, Tyr, Oct, Gly and L-DOPA). The inset shows
1261 the normalized dose-dependent fluorescence responses of GRAB_{DA1m}-
1262 expressing cells in response to DA (red) and NE (green) application ($n = 6$ wells
1263 per group with 100-300 cells per well; $p = 0.002$ at -7.5; $p < 0.001$ at -7, -6.5
1264 and -6; $p = 0.007$ at -5).

1265 (I) Normalized fluorescence changes in GRAB_{DA}-expressing cells in response
1266 to the application of DA, with or without the co-expression of pertussis toxin
1267 (PTX) (GRAB_{DA1m}: $n = 14/3$; GRAB_{DA1m}+PTX: $n = 14/3$; GRAB_{DA1h}: $n = 10/3$;
1268 GRAB_{DA1h}+PTX: $n = 10/3$; $p = 0.680$ comparing the EC₅₀ of GRAB_{DA1m} and
1269 GRAB_{DA1m} +PTX; $p = 0.810$ for comparing the EC₅₀ of GRAB_{DA1h} and GRAB_{DA1h}
1270 +PTX).

1271 (J) Normalized Fluorescence changes in GRAB_{DA}-expressing cells during a 2-
1272 hour application of 100 μ M DA ($n = 3$ wells/group; $p = 0.620$ for GRAB_{DA1m}; $p =$
1273 0.792 for GRAB_{DA1h}).

1274 Scale bars, 10 μ m in (D) and (F).

1275 Values with error bars indicate mean \pm SEM.

1276 Students' t-test performed; n.s., not significant; **, $p < 0.01$; ***, $p < 0.001$.

1277 See also Fig. S1-S3.

1278

1279 **Figure 2. Characterization of GRAB_{DA} sensors in cultured neurons.**

1280 (A) Expression of GRAB_{DA} sensors in cultured neurons. Scale bars, 20 μ m.

1281 (B) Expression and localization of GRAB_{DA} sensors (green, G), subcellular
1282 markers (red, R) and overlay (O) in the indicated subcellular compartments in
1283 cultured neurons. RFP-CAAX, PSD95-RFP and Synaptophysin-RFP were co-
1284 expressed as markers of the plasma membrane, dendritic spines, and
1285 presynaptic boutons, respectively. Scale bars, 5 μ m.

1286 (C and D) Fluorescence changes in GRAB_{DA}-expressing neurons in response
1287 to the application of 100 μ M DA followed by 10 μ M Halo. Scale bars, 30 μ m
1288 (GRAB_{DA1m}: $n = 13/7$; GRAB_{DA1m-mut}: $n = 14/5$; GRAB_{DA1h}: $n = 16/4$; GRAB_{DA1h-}
1289 mut : $n = 10/5$; $p < 0.001$ between DA1m and DA1m-mut; $p < 0.001$ between
1290 DA1h and DA1h-mut; $p = 0.88$ between DA1m and DA1h).

1291 (E) Time courses (left) and dose-dependent fluorescence changes (right) of
1292 GRAB_{DA}-expressing neurons in response to DA application (GRAB_{DA1m}: $n =$
1293 $10/6$; GRAB_{DA1m-mut}: $n = 6/6$; GRAB_{DA1h}: $n = 10/5$; GRAB_{DA1h-mut}: $n = 10/3$).

1294 (F) Fluorescence changes in GRAB_{DA1m}-expressing neurons in response to the
1295 transient application of the indicated compounds at 1 μ M, including DA, L-Dopa,
1296 5-HT, His, ACh, DA(2nd) and DA+Halo ($n = 12/12$; $p < 0.001$ comparing
1297 responses in DA with that in L-Dopa, 5-HT, His, ACh and DA+Halo).

1298 (G) Fluorescence changes in GRAB_{DA}-expressing neurons during a 2-hour
1299 application of 100 μ M DA (GRAB_{DA1m}: $n = 20/12$; GRAB_{DA1h}: $n = 14/6$; $p = 0.085$
1300 for DA1m; $p = 0.085$ for DA1h).

1301 Values with error bars indicate mean \pm SEM.

1302 Student's t-test performed; n.s., not significant; ***, $p < 0.001$.

1303 See also Fig. S4.

1304 **Figure 3. Release of endogenous DA measured in acute mouse brain**
1305 **slices.**

1306 (A) Left three panels, schematic diagrams of the viral expression vector,
1307 experimental protocol for expressing GRAB_{DA} sensors and imaging DA
1308 dynamics in mouse brain slices containing NAc. Right, the immunoreactive
1309 signals of GRAB_{DA} (green) expressed in NAc neurons and TH (red) in
1310 dopaminergic terminals. Scale bar, 100 μ m.

1311 (B) Representative traces (left and middle) and group analysis (right) of the
1312 fluorescence changes in GRAB_{DA1m}- and GRAB_{DA1h}-expressing neurons in
1313 response to a train of 20 Hz electrical stimuli containing the indicated pulse
1314 numbers. Each trace is the average of 3 separate trials in one slice (GRAB_{DA1m}:
1315 $n = 5$ slices from 3 mice; GRAB_{DA1h}: $n = 7$ slices from 4 mice).

1316 (C) Similar as (B), except that a train of 10-pulse electrical stimuli was applied
1317 at the indicated frequencies (GRAB_{DA1m}: $n = 3$ slices from 2 mice; GRAB_{DA1h}: n
1318 = 8 slices from 4 mice).

1319 (D) Representative traces (left) and group analysis (right) of the normalized
1320 fluorescence changes and kinetics in GRAB_{DA1m}- and GRAB_{DA1h}-expressing
1321 neurons in response to 10 electrical pulses delivered at 100 Hz. The rising (on)
1322 and decaying (off) phases in the traces were fitted separately, and the response
1323 time constants are summarized on the right (GRAB_{DA1m}: $n = 3$ slices from 2
1324 mice; GRAB_{DA1h}: $n = 5-8$ slices from 3 mice).

1325 (E) The fluorescence changes in GRAB_{DA1m}- and GRAB_{DA1h}-expressing
1326 neurons in response to multiple trains of electrical stimuli at an interval of 5 min.
1327 The fluorescence changes measured during the first train in each slice were
1328 used to normalize the data (GRAB_{DA1m}: $n = 3$ slices from 2 mice; GRAB_{DA1h}: n
1329 = 6 slices from 3 mice).

1330 (F) Representative traces (left and middle) and group analysis (right) of the
1331 fluorescence changes in GRAB_{DA1m}- and GRAB_{DA1h}-expressing neurons in
1332 response to 20 electrical pulses (at 20 Hz), in control solution (ACSF) or
1333 solution containing 10 μ M Halo (GRAB_{DA1m}: $n = 5$ slices from 4 mice, $p < 0.001$
1334 comparing ACSF with Halo; GRAB_{DA1h}: $n = 6$ slices from 4 mice, $p < 0.001$
1335 comparing ACSF with Halo).

1336 Values with error bars indicate mean \pm SEM.

1337 The shaded areas and error bars indicate \pm SEM.

1338 Student's t-test performed; ***, $p < 0.001$.

1339

1340 **Figure 4. *In vivo* imaging of DA dynamics in the *Drosophila* brain.**

1341 (A) Schematic illustration depicting the *in vivo* olfactory stimulation and imaging
1342 experiment under two-photon microscopy.

1343 (B and C) Representative pseudo-color images and traces (B) and group
1344 analysis (C) of the fluorescence changes of TH > GRAB_{DA1m} and TH >
1345 GRAB_{DA1m-mut} flies in response to 1 s olfactory stimulation (TH > GRAB_{DA1m}: *n*
1346 = 12 flies; TH > GRAB_{DA1m-mut}: *n* = 5 flies; c305a > GRAB_{DA1m} with WT
1347 background: *n* = 6 flies; c305a > GRAB_{DA1m} with TH-deficient background: *n* =
1348 6 flies; *p* < 0.001 for responses of TH > GRAB_{DA1m} in saline comparing with
1349 Halo; *p* < 0.001 for responses of TH > GRAB_{DA1m} in saline comparing with TH >
1350 GRAB_{DA1m-mut} in saline; *p* = 0.002 for responses of c305a > GRAB_{DA1m} with WT
1351 background comparing with TH-deficient background).

1352 (D) Schematic illustrations depicting *in vivo* electrical stimulation experiment, in
1353 which the electrode was positioned near the GRAB_{DA1m}-expressing DANs in
1354 order to evoke DA release.

1355 (E) Representative pseudo-color images of the fluorescence changes in TH >
1356 GRAB_{DA1m} and TH > GRAB_{DA1m-mut} flies in response to multiple trains of
1357 electrical stimuli. Shown below are single-trial traces (in gray) and 6-trial
1358 averaged traces (blue and black) measured in one fly with indicated genotypes.
1359 Each vertical tick indicates 1 ms electrical stimulation (“stim”).

1360 (F-I) Fluorescence changes in TH > GRAB_{DA1m} flies in response to the indicated
1361 pulses of electrical stimuli (at 20 Hz), showing representative traces (F), group
1362 data for peak $\Delta F/F_0$ (G), integrated data (H) and the response kinetics (I) (*n* = 9
1363 flies per group).

1364 (J and K) Representative traces (J) and group analysis (K) of fluorescence
1365 changes in TH > GRAB_{DA1m} and TH > GRAB_{DA1m-mut} flies in response to 40
1366 pulses electrical stimuli (at 20 Hz), in normal saline or in saline containing 10
1367 μ M Halo (TH > GRAB_{DA1m}: *n* = 5 flies; TH > GRAB_{DA1m-mut}: *n* = 5 flies; *p* = 0.004
1368 for responses of TH > GRAB_{DA1m} in saline comparing with Halo; *p* = 0.007 for
1369 responses of TH > GRAB_{DA1m} in saline comparing with TH > GRAB_{DA1m-mut} in
1370 saline).

1371 (L-O) Fluorescence changes in TH > GRAB_{DA1m} flies in response to 1 s olfactory
1372 stimulation, in control condition, in the presence of the DAT blocker cocaine (3
1373 μ M) or when the DAT expression in DAN was impaired by DAT-RNAi.
1374 Schematic illustration of the experimental design in (L). Representative traces
1375 (M) were fitted with a single-exponential function (red traces), with the decay
1376 time constants shown. The group analysis of integrated data and the decay
1377 time constants are shown in (N) and (O), respectively (TH > GRAB_{DA1m}: *n* = 10

1378 flies; TH > GRAB_{DA1m}, DAT-RNAi: $n = 11$ flies; between control and cocaine
1379 groups, $p = 0.002$ for integrals and $p = 0.025$ for decay time constants; between
1380 control and DAT-RNAi groups, $p < 0.001$ for both integrals and decay time
1381 constants; between cocaine and DAT-RNAi groups, $p = 0.095$ for integrals and
1382 $p = 0.053$ for decay time constants).

1383 The fluorescence traces in (B), (F), (J), and (M) are the averaged results of 3~6
1384 trials from one fly, and the shaded area indicates \pm SEM.

1385 Values with error bars indicate mean \pm SEM.

1386 Student's t-test performed; n.s., not significant; *, $p < 0.05$; **, $p < 0.01$; ***, $p <$
1387 0.001.

1388 Scale bars in (B) and (E), 25 μm .

1389 See also Fig. S5.

1390

1391

1392 **Figure 5. Monitoring *in vivo* DA release in transgenic zebrafish.**

1393 (A) Fluorescence images of a transgenic zebrafish larvae expressing
1394 GRAB_{DA1m} (green) pan-neuronally and TRPV1-TagRFP (red) in DANs. Zoom-
1395 in view of GRAB_{DA1m}-expressing neurons in indicated brain regions are shown
1396 (left).

1397 (B-D) Representative pseudo-color images (B), trace (C) and group analysis (D)
1398 of fluorescence changes of GRAB_{DA1m}-expressing neurons in response to 100
1399 μ M DA followed by 50 μ M Halo ($n = 6$ fishes; $p = 0.002$ between DA and
1400 DA+Halo).

1401 (E) Schematic diagram showing the experimental design to chemogenetically
1402 activate TRPV1-expressing DANs by capsaicin. The tectal neurons
1403 downstream of the DANs were analyzed as indicated by the region of interest
1404 (ROI).

1405 (F) Representative traces of the fluorescence changes in GRAB_{DA1m}-
1406 expressing neurons in response to 5 pulses of 50 μ M capsaicin (each vertical
1407 orange tick indicates 100-ms puffs of capsaicin with a 1 min interval) in control
1408 normal solution (green) or solution containing 50 μ M Halo (blue).

1409 (G and H) Averaged traces (G) and group analysis (H) of the fluorescence
1410 changes in GRAB_{DA1m}-expressing neurons in response to single trial of
1411 capsaicin application, in control normal solution (green) or solution containing
1412 50 μ M Halo (blue) ($n = 5$ fishes; $p = 0.006$ between control and Halo).

1413 Scale bars in (A) and (B), 50 μ m.

1414 Paired student's t-test performed.

1415

1416 **Figure 6. Striatal DA dynamics measured in freely moving mice during**
1417 **optogenetic stimulation of the SNc.**

1418 (A) Illustration depicting the experimental design with dual-color optical
1419 recordings of GRAB_{DA1m}- and tdTomato-expressing neurons in the dorsal
1420 striatum during simultaneous optogenetic stimulation of DANs in the SNc.

1421 (B) A representative frame of the emission spectra of GRAB_{DA1m} and tdTomato
1422 co-expressed in the dorsal striatum. The black trace shows the measured
1423 spectrum; the blue dashed trace shows the corresponding best fitting curve
1424 generated by a linear unmixing algorithm.

1425 (C) Spontaneous DA fluctuations represented by the ratio of GRAB_{DA1m} to
1426 tdTomato fluorescence in a freely moving mouse (top) and its representative
1427 traces in the control condition (bottom left), 5 min after the i.p. injection of DAT
1428 blocker methylphenidate (10 mg/kg, bottom middle), and 5 min after the i.p.
1429 injection of D₂R antagonist Etic (2 mg/kg, bottom right). Black lines above
1430 indicate the time of compound administration. Yellow ticks indicate the time of
1431 optogenetic stimulation.

1432 (D) Averaged fluorescence changes (mean \pm SEM, $n = 20$ trials from 4
1433 hemispheres of 2 mice) of GRAB_{DA1m} (green) in the dorsal striatum in response
1434 to optogenetic C1V1 stimulation of DANs in the SNc under indicated conditions:
1435 baseline (left), after the i.p. injection of methylphenidate (middle), and after the
1436 i.p. injection of Etic (right). The off kinetics were fitted with a single-exponential
1437 function (black traces).

1438 (E) Comparison of the decay time constants of C1V1-evoked GRAB_{DA1m}
1439 fluorescence responses between the control condition and after
1440 methylphenidate injection ($n = 20$ trials from 4 hemispheres of 2 mice).

1441 (F) Comparison of the magnitude of C1V1-evoked GRAB_{DA1m} fluorescence
1442 changes between the control condition and after Etic injection ($n = 20$ trials from
1443 4 hemispheres of 2 mice).

1444 *******, $p < 0.001$, student's t-test performed in (E) and (F).

1445

1446 **Figure 7. Dopamine release in NAc measured during various training**
1447 **phases of an auditory conditioning task.**

1448 (A) Recording configuration for head-fixed Pavlovian conditioning task.
1449 Dopamine dynamics in the NAc were monitored by recording the fluorescence
1450 changes in GRAB_{DA}-expressing neurons using fiber photometry.

1451 (B) Exemplar trace from *in vivo* fiber photometry recording from a trained mouse
1452 expressing GRAB_{DA1h} in NAc, encompassing four sequential trials. The timings
1453 of cues (CS) or water reward (US) are indicated above.

1454 (C) Task-aligned photometry signals from an exemplar mouse in the first
1455 behavioral session aligned to the cue (CS, left) or to the reward delivery (US,
1456 right). Note robust reward-related signal and absence of cue-related signal.

1457 (D) Task-aligned photometry signals from the same mouse in (C) after training.
1458 Note emergence of DA response to reward-predictive cue.

1459 (E) Group data demonstrating GRAB_{DA1h} responses to water (US, left) or cue
1460 (CS, middle) in the NAc of both naïve and trained mice ($n = 9$ mice; US
1461 response: naïve N.W.: $p = 0.084$; naïve water: $p = 0.0020$; trained N.W.: $p =$
1462 0.56 ; trained water: $p = 0.0020$; CS response: naïve N.W.: $p = 0.37$; naïve water:
1463 $p = 1.0000$; trained N.W.: $p = 0.043$; trained water: $p = 0.0020$, signed rank test
1464 performed).

1465 (F) Direct comparison of baseline-subtracted cue responses reveals equivalent
1466 lack of response to N.W. or reward-predictive cue in naïve mice (left), and
1467 elevated response to reward-predictive cue over N.W. cue in trained mice (right).
1468 Baseline subtraction was performed trial-by-trial by comparing the cue
1469 response (100 ms – 1000 ms following onset of the cue) to 900 ms before onset
1470 of the cue. This cue response window encompassed the auditory cue as well
1471 as the variable delay period and terminated before the earliest reward delivery
1472 times (naïve: $p = 0.43$; trained: $p = 0.0020$, signed rank test performed).

1473 (G) Representative fluorescence changes in GRAB_{DA1m}-expressing neurons in
1474 the NAc during training. The heat map shows the fluorescence changes in the
1475 first 50 consecutive trials in each category, with each trial time-aligned to the
1476 onset of the auditory cue. The lower panels show the post-event histograms
1477 (PSTH) from all trials; the shaded area indicates \pm SD. The fluorescence
1478 changes measured during naïve, trained and well-trained phases in the same
1479 mouse are shown, respectively.

1480 (H) Group analysis of the normalized peak z-scores for the US and CS in the
1481 indicated training phases. Each trace (coded with specific gray value)
1482 represents data from one animal ($n = 3$ mice; US: $p = 0.7638$ between naïve

1483 and trained, $p = 0.0125$ between naive and well-trained, $p = 0.0080$ between
1484 trained and well-trained; CS: $p = 0.1032$ between naive and trained, $p = 0.0067$
1485 between naive and well-trained, $p = 0.0471$ between trained and well-trained).
1486 Error bars, \pm SEM. Post-hoc Tukey's test was performed; n.s., not significant; *,
1487 $p < 0.05$; **, $p < 0.01$; ***, $p < 0.001$.

1488

1489 **Figure 8. Acute DA release in the NAc measured during male sexual**
1490 **behaviors.**

1491 (A) Schematic diagram showing the experimental design used to record
1492 GRAB_{DA1h} signals in the NAc of male mice during sexual behaviors.

1493 (B) Representative fluorescence changes in male mice during the indicated
1494 sexual behaviors. The shaded areas with colors indicate different behavioral
1495 events.

1496 (C) Post-event histogram (PETH) showing the GRAB_{DA1h} signals aligned to the
1497 indicated behavioral events.

1498 (D) Group data summarizing the average peak $\Delta F/F_0$ (baseline adjusted) during
1499 different indicated behaviors for the two mice shown in (C) ($n = 2$ mice; $p =$
1500 0.007 for animal 1; $p < 0.001$ for animal 2). Error bars, \pm SEM. One-way ANOVA
1501 performed; ***, $p < 0.001$; **, $p < 0.01$.

Figure 1

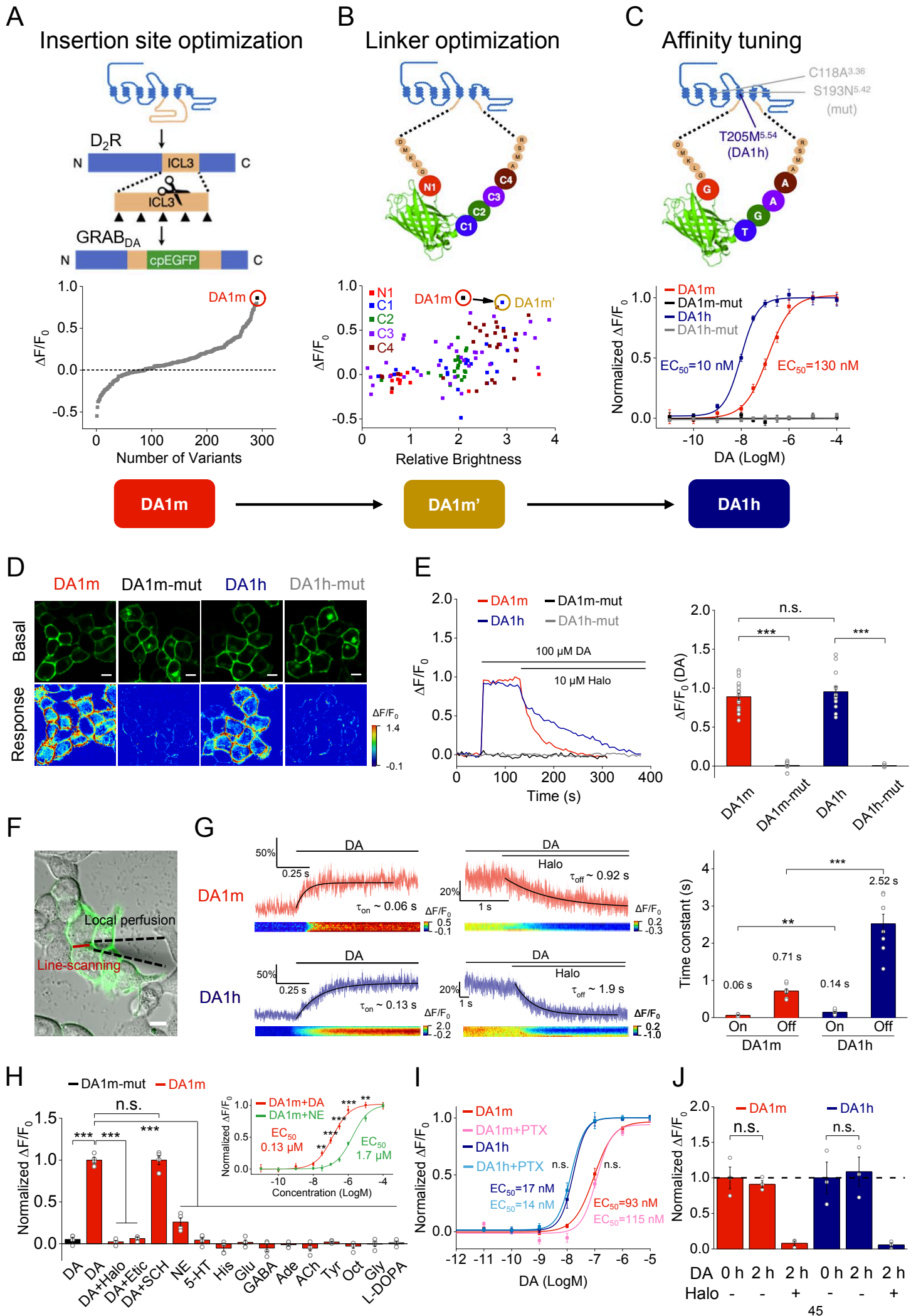


Figure 2

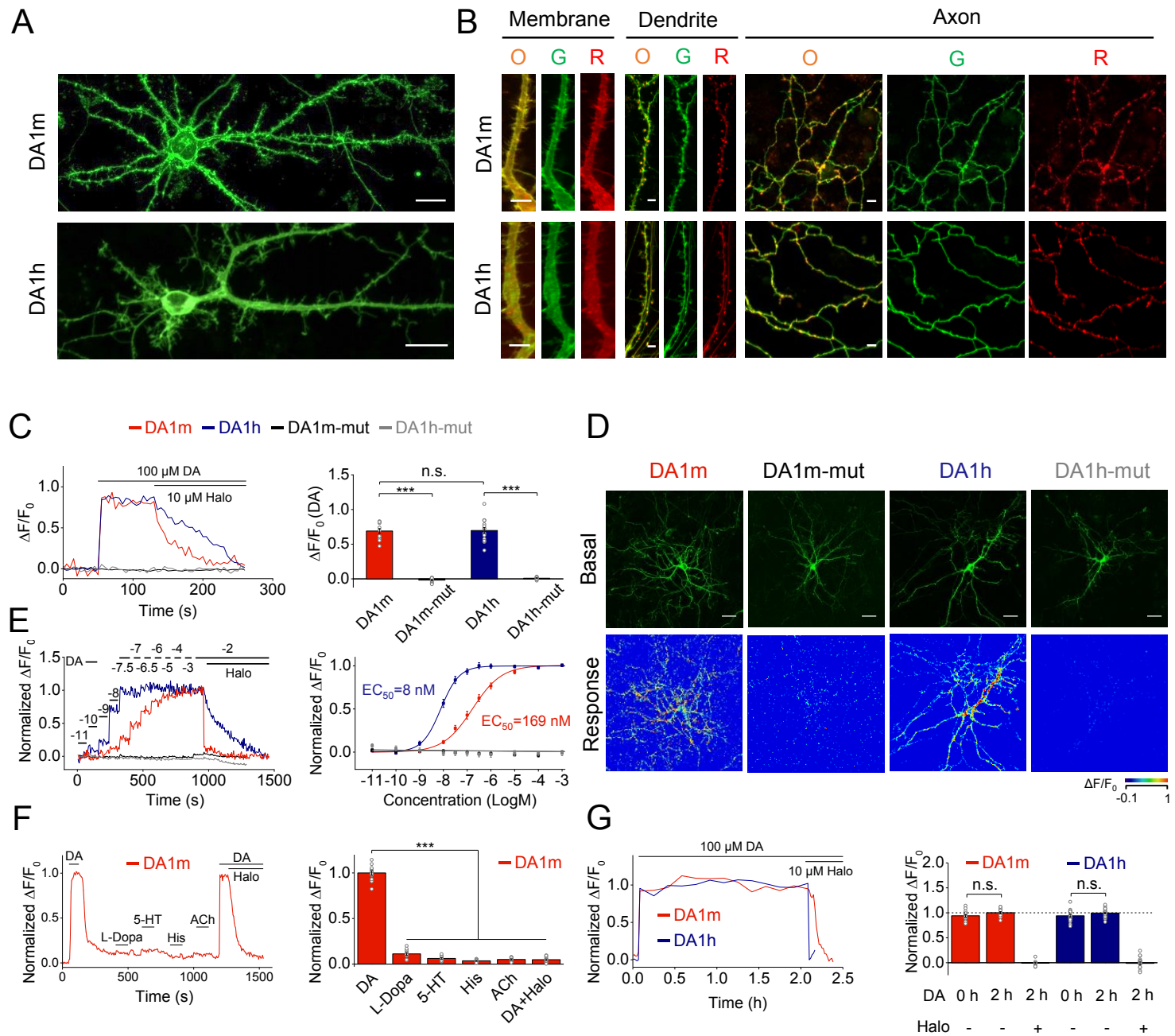


Figure 3

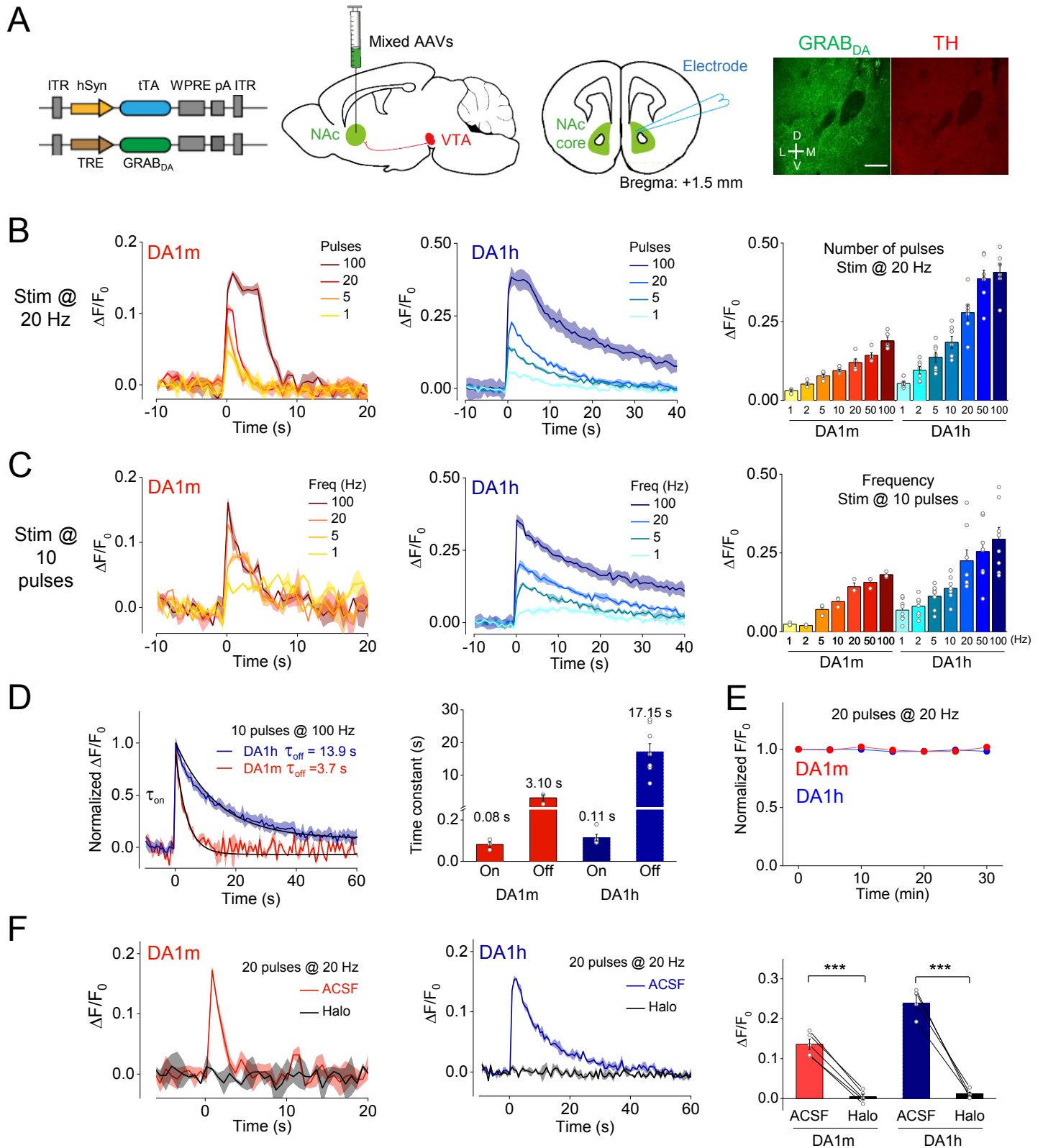


Figure 4

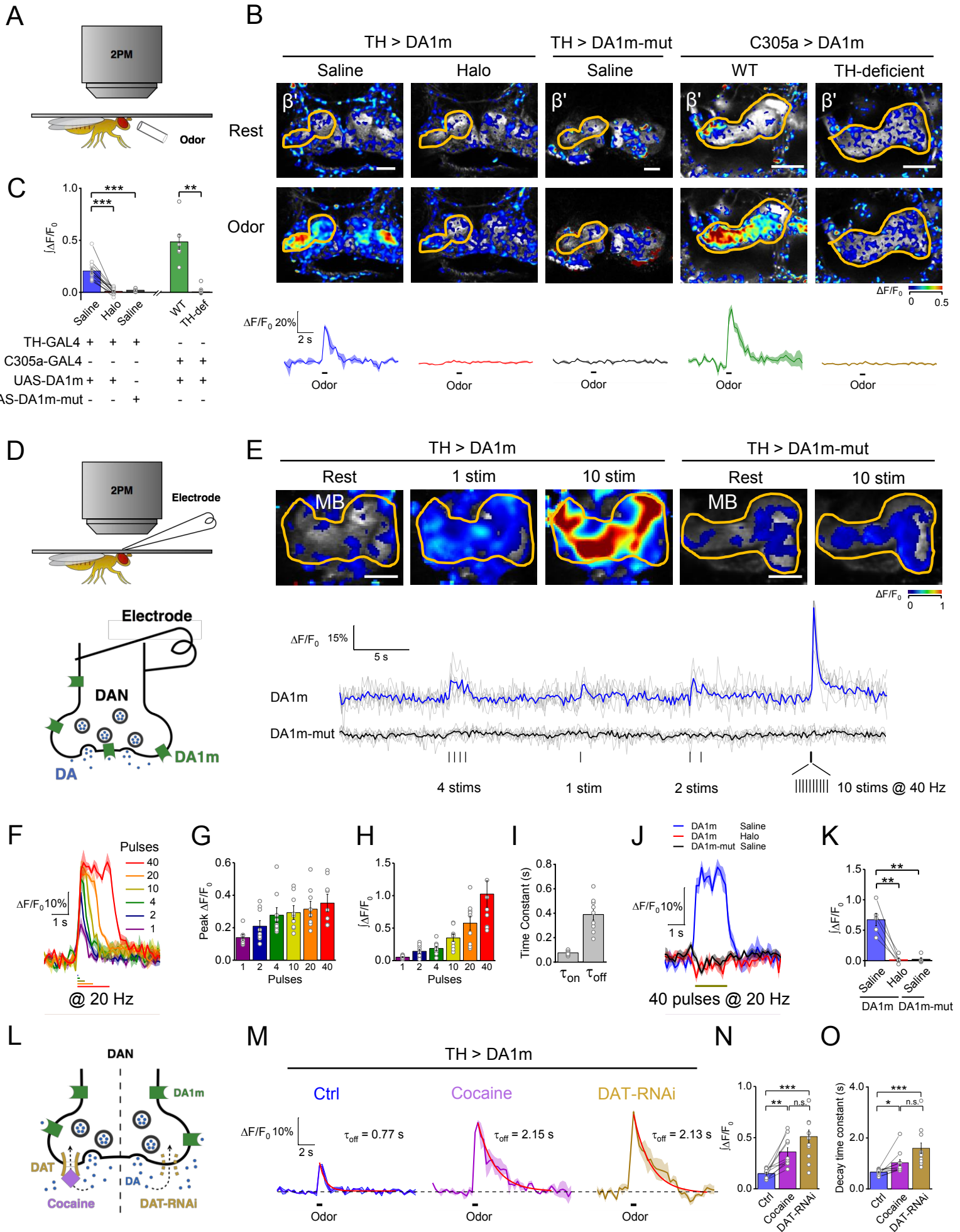


Figure 5

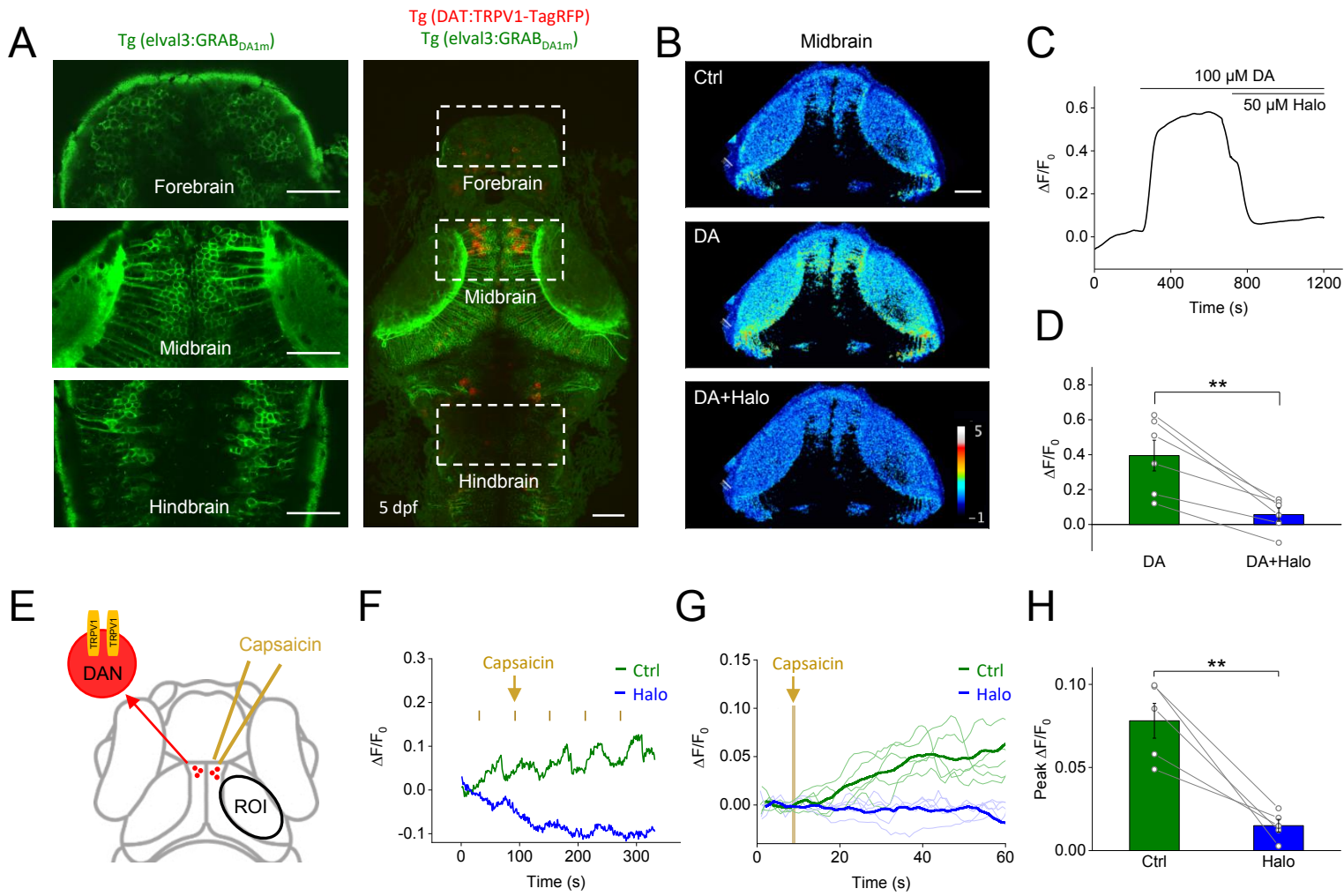


Figure 6

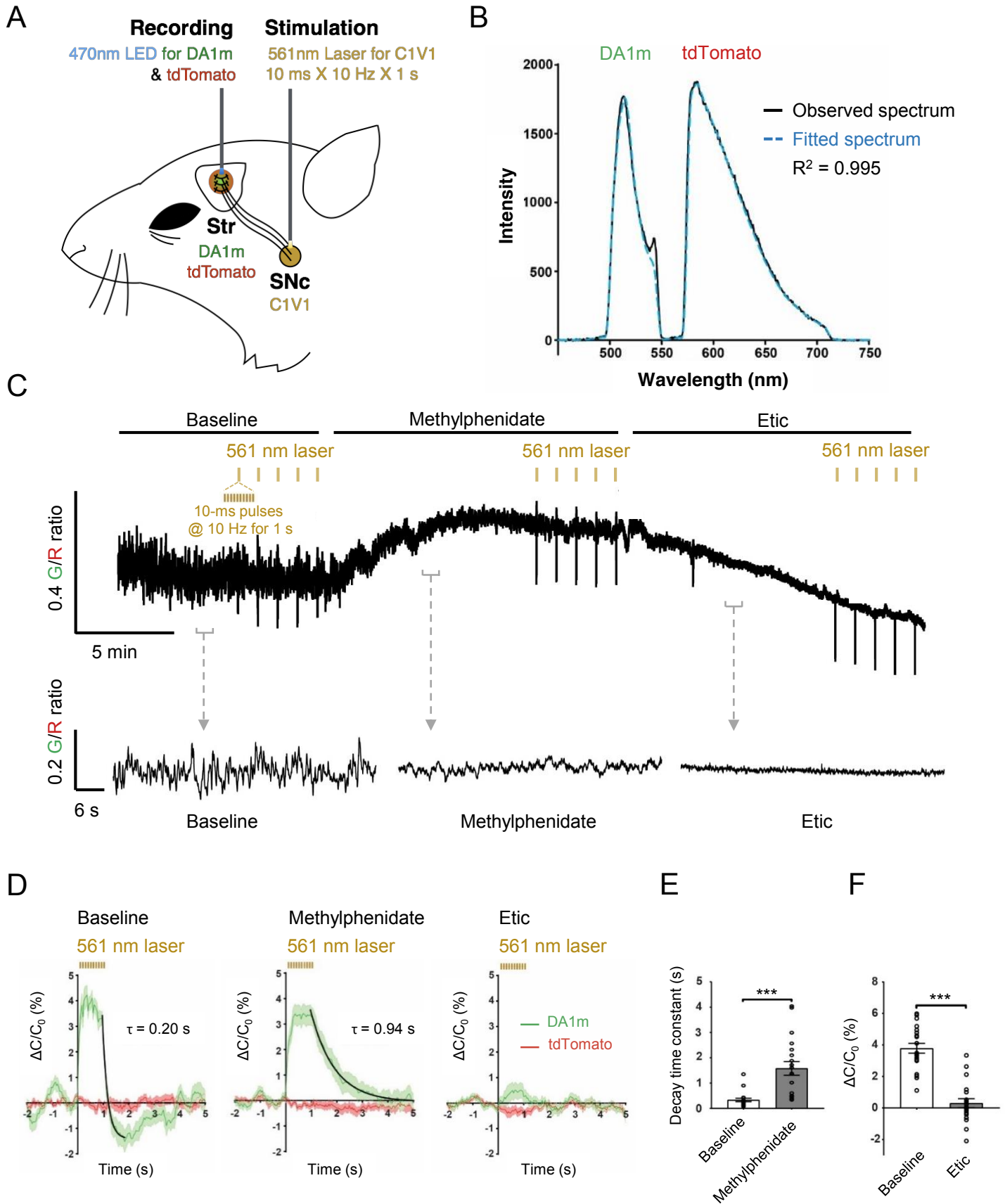


Figure 7

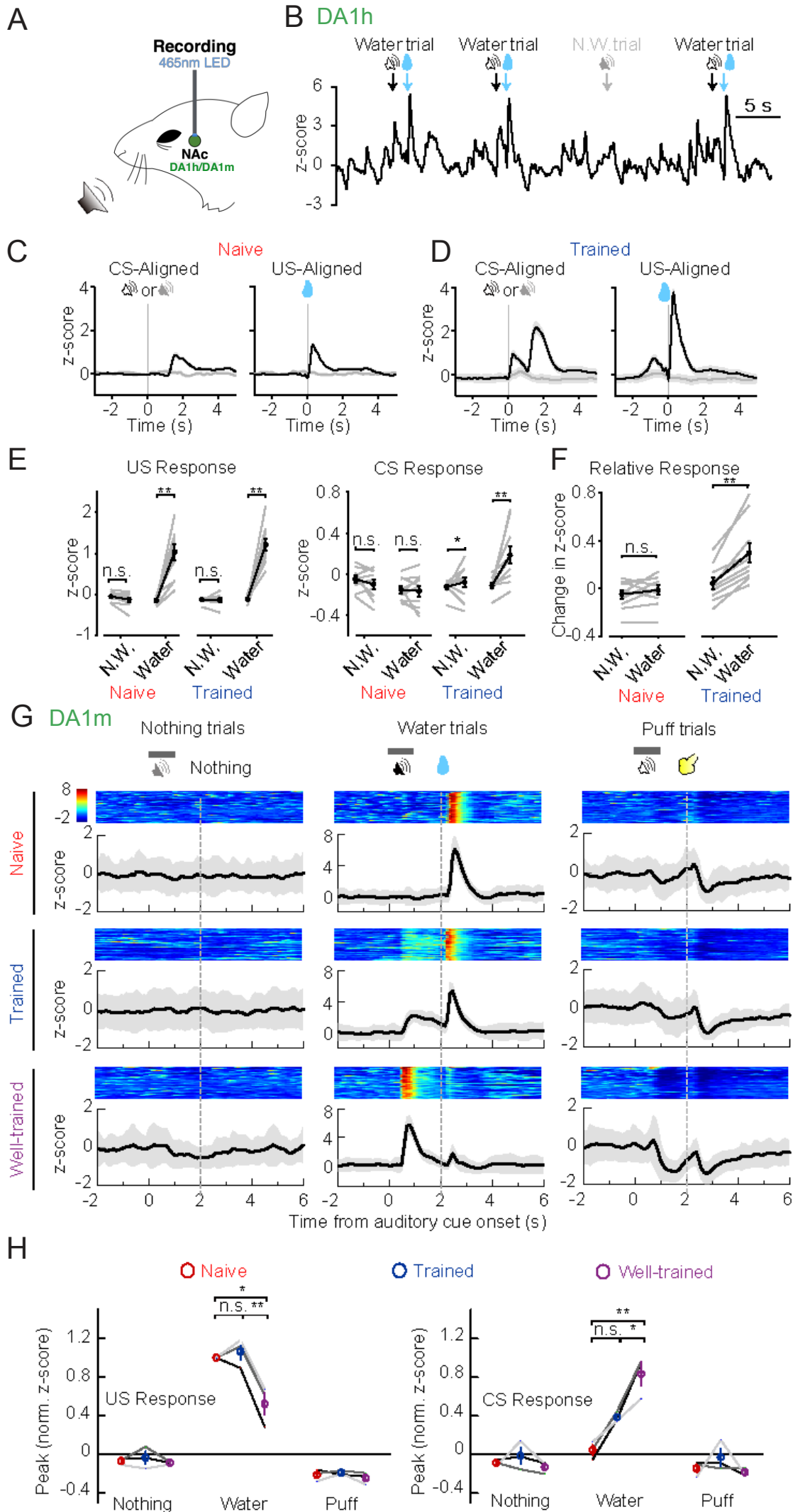
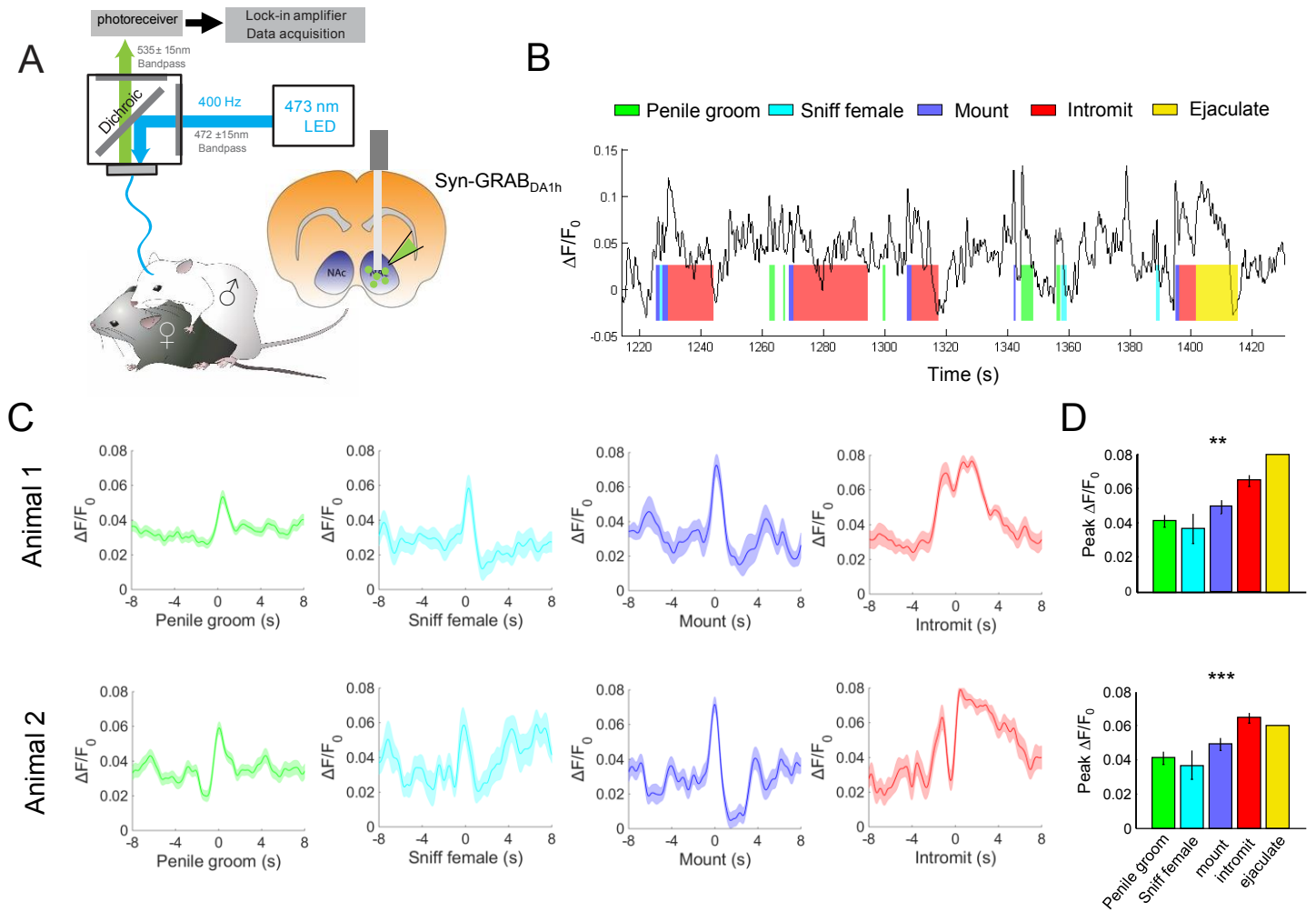


Figure 8



1502 **Figure S1: Comparison of DRs and DR-based chimeras, related to Fig. 1.**

1503 (A) The fluorescence and membrane trafficking of all five DRs with cpEGFP
1504 insertion. A membrane localized RFP (RFP-CAAX) was co-expressed to
1505 indicate the plasma membrane and EGFP-CAAX was set as a control. Left, the
1506 fluorescence images of HEK293T cells expressing all five DR-based chimeras
1507 (green) and RFP-CAAX (red). Middle, the normalized line-scanning plots of the
1508 fluorescence signals in both green and red channels. Right, Pearson
1509 colocalization ratios between the DR-based chimeras and RFP-CAAX ($n = 30/2$
1510 for each protein; $p < 0.001$ comparing D₂R with D₃R, D₄R and D₅R; $p = 0.001$
1511 between D₂R and EGFP-CAAX; $p = 0.006$ between D₂R and D₁R).

1512 (B) DA binding affinities of five subtypes of DRs.

1513 (C) Similar as (A), except different D₂R based GRAB_{DA} sensors were
1514 characterized, including GRAB_{DA1m}, GRAB_{DA1m-mut}, GRAB_{DA1h}, GRAB_{DA1h-mut}
1515 and Golgi marker KDELR1-GFP as a control ($n = 30/2$ for each protein; $p > 0.05$
1516 among GRAB_{DA} sensors; $p < 0.001$ comparing KDELR1 with GRAB_{DA} sensors).

1517 (D) Sequence alignment of the binding pockets of D₁R-D₅R and D₂R-based
1518 GRAB_{DA} sensors. Two blue-shaded amino acids indicate C118A and S193N
1519 mutation sites.

1520 Scale bars in (A) and (C), 10 μ m.

1521

1522 **Figure S2: Photostability of GRAB_{DA1m} and GRAB_{DA1h} compared with**
1523 **other fluorescent probes, related to Fig. 1.**

1524 (A) Representative photobleaching curves of GRAB_{DA1m}, GRAB_{DA1h}, EGFP-
1525 CAAX and iGluSnFR expressed in HEK293T cells under confocal imaging
1526 (488 nm laser with ~350 μ W intensity).

1527 (B) The group data of fluorescence decrease time constants of GRAB_{DA1m},
1528 GRAB_{DA1h}, EGFP-CAAX and iGluSnFR ($n = 10/3$; $p = 0.350$ between
1529 GRAB_{DA1m} and GRAB_{DA1h}; $p < 0.001$ comparing GRAB_{DA1m} with EGFP-CAAX
1530 and iGluSnFR).

1531

1532 **Figure S3: The selectivity of GRAB_{DA1h}, related to Fig. 1.**

1533 Normalized fluorescence responses of GRAB_{DA1h}- or GRAB_{DA1h-mut}-expressing
1534 cells to the application of 1 μ M different compounds, including: DA, DA with
1535 Halo, DA with Etic, DA with SCH, 5-HT, His, Glu, GABA, Ade, ACh, Tyr, Oct, Gly
1536 and L-Dopa (the first bar shows GRAB_{DA1h-mut}-expressing cells in response to
1537 DA; $n = 3$ wells with each well of 200-400 cells; $p < 0.001$ for DA-induced
1538 responses between GRAB_{DA1h} and GRAB_{DA1h-mut}; $p = 0.66$ for GRAB_{DA1h}
1539 responses induced by DA comparing with DA+SCH; $p = 0.037$ for GRAB_{DA1h}
1540 responses induced by DA comparing with NE; $p < 0.001$ for GRAB_{DA1h}
1541 responses induced by DA comparing with DA+Halo, DA+Etic, 5-HT, His, Glu,
1542 GABA, Ade, ACh, Tyr, Oct, Gly and L-DOPA). The inset, normalized dose-
1543 dependent fluorescence responses of GRAB_{DA1h}-expressing cells to the
1544 application of DA (blue) or NE (orange) ($n = 6$ wells with each well of 200-400
1545 cells; $p < 0.001$ at -8, -7.5, -7 and -6.5; $p = 0.049$ at -6).

1546

1547 **Figure S4: Expression and membrane trafficking of GRAB_{DA1m-mut} and**
1548 **GRAB_{DA1h-mut} in cultured neurons, related to Fig. 1.**

1549 The fluorescence images of GRAB_{DA1m-mut}- and GRAB_{DA1h-mut}-expressing
1550 neurons under confocal microscope. RFP-CAAX was co-expressed in the
1551 same neuron to indicate the plasma membrane. Scale bars of whole views, 20
1552 μm . Scale bars of zoom-in views, 5 μm .

1553

1554 **Figure S5: GRAB_{DA1m} expression has no effect on the odor-evoked Ca²⁺**
1555 **signaling, related to Fig. 4.**

1556 (A) The schematic of *in vivo* olfactory stimulation experiment under two-photon
1557 microscope.

1558 (B) Representative pseudo-color images and traces of fluorescence responses
1559 of jRCaMP1a-expressing DANs (left) or Kenyon cells (right) to 1 s olfactory
1560 stimulation. Traces are 3-trial-averaged results from one fly, and are shaded
1561 with \pm SEM. Scale bars, 25 μ m.

1562 (C) The integrals of jRCaMP1a signals are summarized. Each dot represents
1563 data from one fly (TH > jRCaMP1a: $n = 10$ flies; TH > jRCaMP1a, GRAB_{DA1m}:
1564 $n = 11$ flies; 30y > jRCaMP1a: 11 flies; 30y > jRCaMP1a, GRAB_{DA1m}: $n = 12$
1565 flies; $p = 0.503$ between TH > jRCaMP1a and TH > jRCaMP1a, GRAB_{DA1m}; $p =$
1566 0.097 between 30y > jRCaMP1a between 30y > jRCaMP1a, GRAB_{DA1m}). Error
1567 bars, \pm SEM. Student's t-test is performed; n.s., not significant.

Figure S2

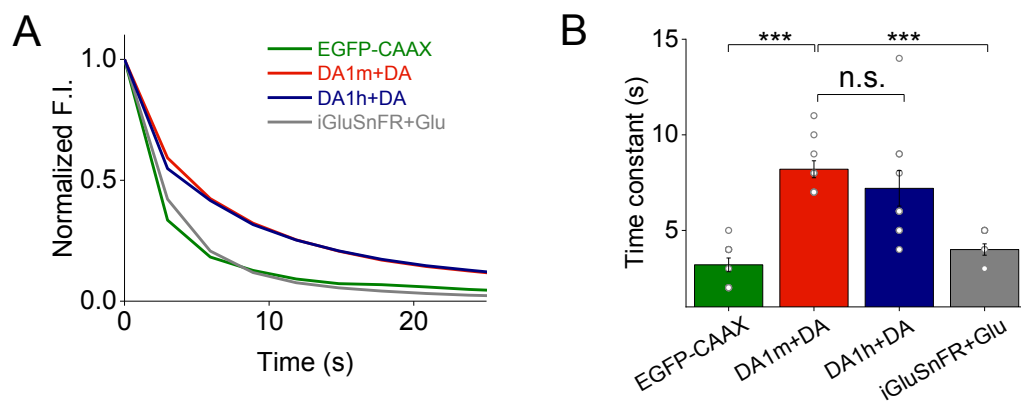


Figure S3

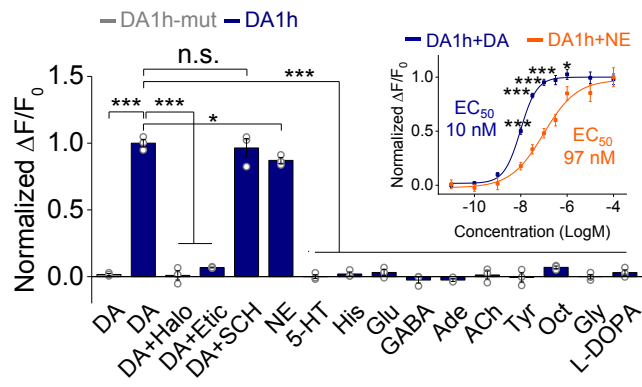


Figure S4

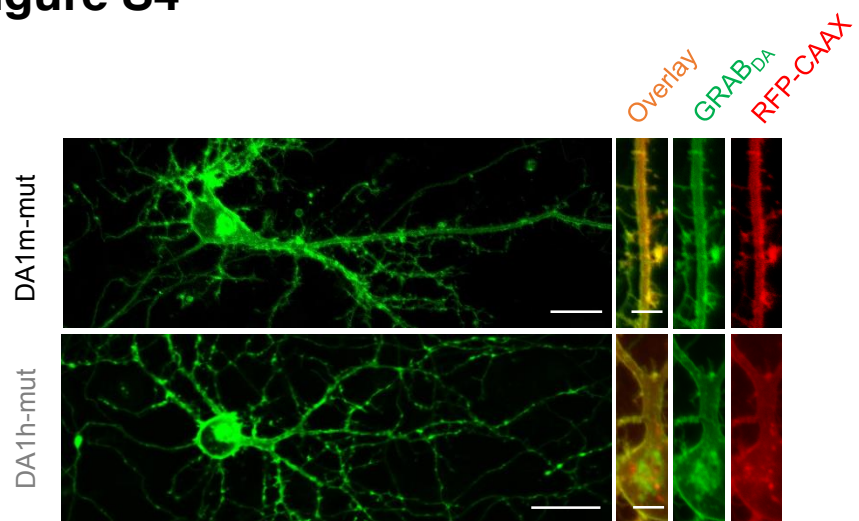


Figure S5

